Research Paper

Cx26 partial loss causes accelerated presbycusis by redox imbalance and dysregulation of Nfr2 pathway

Anna Rita Fetoni[a,b,c,1], Veronica Zorzi[a,b,1], Fabiola Paciello[a,b,1], Gaia Ziraldo[a,b], Chiara Peres[a], Marcello Raspa[a], Ferdinando Scavizzi[a], Anna Maria Salvatore[a], Giulia Crispino[a], Gabriella Tognola[d], Giulia Gentile[e], Antonio Gianmaria Spampinato[e], Denis Cuccaro[e], Maria Guarnaccia[e], Giovanna Morello[e], Guy Van Camp[f], Erik Fransen[g], Marco Brumat[h,i], Giorgia Girotto[h,i], Gaetano Paludetti[b,c], Paolo Gasparini[h,i,*], Sebastiano Cavallaro[e,**], Fabio Mammano[a,j,***]

[a] CNR Institute of Cell Biology and Neurobiology, Monterotondo 00015, Italy
[b] Università Cattolica del Sacro Cuore, Largo F. Vito 1, 00168 Rome, Italy
[c] Institute of Otolaryngology, Fondazione Policlinico Universitario A. Gemelli IRCCS, Largo F. Vito 1, 00168 Rome, Italy
[d] CNR Institute of Electronics, Computer and Telecommunication Engineering, 20133 Milano, Italy
[e] CNR Institute of Neurological Sciences, 95126 Catania, Italy
[f] Center of Medical Genetics, University of Antwerp and Antwerp University Hospital, Universiteitsplein 1, 2610 Antwerp, Belgium
[g] Department of Biomedical Sciences, University of Antwerp, 2650 Antwerp, Belgium
[h] Dept Med Surg & Hlth Sci, University of Trieste, Trieste, Italy
[i] IRCCS Burlo Garofolo, Inst Maternal & Child Hlth, Trieste, Italy
[j] University of Padova, Department of Physics and Astronomy "G. Galilei", Padova, Italy

A B S T R A C T

Mutations in *GJB2*, the gene that encodes connexin 26 (Cx26), are the most common cause of sensorineural hearing impairment. The truncating variant 35delG, which determines a complete loss of Cx26 protein function, is the prevalent *GJB2* mutation in several populations. Here, we generated and analyzed $Gjb2^{+/-}$ mice as a model of heterozygous human carriers of 35delG. Compared to control mice, auditory brainstem responses (ABRs) and distortion product otoacoustic emissions (DPOAEs) worsened over time more rapidly in $Gjb2^{+/-}$ mice, indicating they were affected by accelerated age-related hearing loss (ARHL), or presbycusis. We linked causally the auditory phenotype of $Gjb2^{+/-}$ mice to apoptosis and oxidative damage in the cochlear duct, reduced release of glutathione from connexin hemichannels, decreased nutrient delivery to the sensory epithelium via cochlear gap junctions and deregulated expression of genes that are under transcriptional control of the nuclear factor erythroid 2-related factor 2 (Nrf2), a pivotal regulator of tolerance to redox stress. Moreover, a statistically significant genome-wide association with two genes (*PRKCE* and *TGFB1*) related to the Nrf2 pathway (p-value $< 4 \times 10^{-2}$) was detected in a very large cohort of 4091 individuals, originating from Europe, Caucasus and Central Asia, with hearing phenotype (including 1076 presbycusis patients and 1290 healthy matched controls). We conclude that (i) elements of the Nrf2 pathway are essential for hearing maintenance and (ii) their dysfunction may play an important role in the etiopathogenesis of human presbycusis.

* Corresponding author at: Dept Med Surg & Hlth Sci, University of Trieste, Trieste, Italy.
** Corresponding author at: CNR Institute of Neurological Sciences, Via P. Gaifami 18, 95126 Catania, Italy.
*** Corresponding author at: CNR Institute of Cell Biology and Neurobiology, Via E. Ramarini 32, 00015 Monterotondo, RM, Italy.
E-mail addresses: paolo.gasparini@burlo.trieste.it (P. Gasparini), sebastiano.cavallaro@cnr.it (S. Cavallaro), fabio.mammano@cnr.it (F. Mammano).
[1] Joint first authors.

1. Introduction

Hearing impairment stands out as the most frequently occurring congenital sensory deficit,[2] with an estimated 1 in 650 newborns affected [1]. Variants of the gap junction protein beta-2 (*GJB2*) gene, also known as connexin 26 (*Cx26*),[3] which include more than 340 missense, nonsense, frameshift, insertions and deletions,[4] take the lion share in the spectrum of deafness–related mutations.[5] The overwhelming majority of these mutations cause nonsyndromic autosomal recessive deafness type 1A (DFNB1A, OMIM[6] 220290) [2,3], which accounts for ~ 50% of all autosomal recessive nonsyndromic hearing impairment cases[7] and are responsible for hearing loss ranging from mild to profound [4,5]. In several populations, the prevalent *GJB2* mutation is 35delG [6,7], a truncating variant that determines a complete loss of function for the encoded Cx26 protein, the structure of which has been solved with a 3.5 Å resolution [8]. The non-sensory (epithelial and supporting) cells of the cochlea that express Cx26, together with the transcriptionally co-regulated connexin 30 (Cx30) encoded by the *GJB6* gene [9], form two distinct cellular networks referred to as epithelial and connective tissue gap junction system, respectively [10].

Despite the undisputed correlation between *GJB2* and *GJB6* variants and hearing loss, the exact function of inner ear connexins and their role in etiopathogenesis of deafness remain largely undetermined. Early attempts to address this issue by mimicking the effect of Cx26 loss of function in mice were ill-fated, as global deletion of *Gjb2* results in embryonic lethality due to impaired transplacental uptake of glucose [11]. To overcome this problem, homozygous mice with floxed *Gjb2* exon 2, abbreviated as *Gjb2*$^{loxP/loxP}$, can be crossed either to a tissue-specific Cre driver [12] or to an inducible global Cre deleter [13]. Crossbreeding *Gjb2*$^{loxP/loxP}$ and Tg(Sox10-cre)1Wdr mice [14] yielded viable homozygous offspring with targeted deletion of Cx26 in the epithelial gap junction network of the cochlea, hereafter abbreviated as *Gjb2*$^{-/-}$ and previously referred to as *Cx26*^{Sox10Cre} [15,16]. Here, we examined in greater detail both *Gjb2*$^{-/-}$ mice and their heterozygous *Gjb2*$^{+/-}$ siblings. We report that both have increased levels of oxidative stress in the cochlea. Whereas *Gjb2*$^{-/-}$ mice fail to acquire hearing [16,17], we discovered that *Gjb2*$^{+/-}$ mice are affected by accelerated age-related hearing loss (ARHL), or presbycusis [18,19], as their auditory performance degraded more rapidly over time than in control mice (see Section 3).

Our analyses linked reduced release of glutathione from connexin hemichannels, apoptosis and oxidative damage in the cochlear duct to decreased nutrient delivery to the sensory epithelium via cochlear gap junctions and deregulated expression of genes that are under transcriptional control of Nrf2, a redox-sensitive transcription factor that plays a pivotal role in oxidative stress regulation [20]. In unstressed cells, the Kelch-like ECH-associated protein 1 (KEAP1) and the Cullin-3-dependent E3 Ubiquitin ligase form a complex (PDB: 5NLB)[8] that represses Nrf2 by promoting its ubiquitination and consequent proteasomal degradation. Oxidative stress leads to modification of KEAP1 cysteine residues, reducing ubiquitination of bound Nrf2. Newly synthesized Nrf2 is then capable of translocating to the nucleus, where it induces the expression of an array of antioxidant response element (ARE)–dependent genes, including Heme-oxygenase 1 (*HO-1*), superoxide dismutase (*SOD*), catalase (*CAT*), glutathione synthetase (*GS*), glutathione reductase (*GR*), glutathione peroxidase (*GPX*) and glutathione-S-transferase (*GST*) [21,22].

Based on the analysis of animal models, and thanks to the availability of a very large cohort of human subjects with presbycusis, we decided to investigate further the role of oxidative stress genes using a candidate gene approach [23]. We report here that some of the genes controlled by the Nrf2/ARE pathway are also significantly associated with hearing function and presbycusis in humans.

2. Materials and methods

2.1. Animals and genotyping

Animals were bread and genotyped in the CNR Monterotondo node of the European Mouse Mutant Archive (EMMA) [24], an ESFRI/INF-RAFRONTIER Distributed Research Infrastructure.[9] *Gjb2*$^{loxP/loxP}$ mice (*Gjb2*^{tm1Ugds}/*Gjb2*^{tm1Ugds}; MGI:2183509; EM:00245) [12] and Tg (Sox10-cre)1Wdr mice (MGI:3586900) [14] were backcrossed for more than 10 generations to C57BL/6N mice purchased from Taconic Biosciences[10] (MGI:2164831) and bred at CNR Monterotondo under Specific and Opportunistic Pathogen-Free (SOPF) conditions. C57BL/6N was selected because it is the background strain for the International Mouse Phenotyping Consortium (IMPC, of which CNR Monterotondo is a member), which aims to produce and phenotype knockout mouse lines for 20,000 genes.[11] Genotyping protocols were performed by PCR using the primers previously described [15,16]. Specifically, *Gjb2*$^{-/-}$ mice (*Gjb2*^{tm1Ugds}/*Gjb2*^{tm1Ugds} Tg(Sox10-cre)1Wdr/0; MGI:5297177; EM:11478) were identified by the presence of the two insertions, *loxP* and *Cre*, by PCR on extracted mouse tail tips using the following primers:

*Gjb2*F 5'-TTTCCAATGCTGGTGGAGTG-3',
*Gjb2*R 5'-ACAGAAATGTGTTGGTGATGG-3',
*Cre*F 5'-CATTACCGGTCGATGCA-3',
*Cre*R 5'-GAACCTGGTCGAAATCAG-3'.

Gjb2$^{+/-}$ mice were identified by the presence of *Cre* and *loxP* insertions in one allele of the *Gjb2* gene, whereas *Gjb2*$^{loxP/loxP}$ mice were identified by the (absence of *Cre* and) presence of *loxP* insertion in both alleles of *Gjb2*.

2.2. Gene expression analysis in mouse samples

Total RNA was extracted from cochlear tissue isolated from four biological replicates for both genotypes, *Gjb2*$^{-/-}$ and *Gjb2*$^{loxP/loxP}$, using Qiagen miRNeasy Mini Kit (Qiagen, Hilden, Germay), and its quantity and quality were assessed using the NanoDrop ND-1000 spectrophotometer (Thermo Fisher Scientific, Waltham, MA, USA) and the Agilent 2100 Bioanalyzer microfluidic electrophoresis platform (Agilent Technologies, Rome, Italy), respectively. Gene expression profiles were investigated using the Agilent SurePrint G3 Mouse Gene Expression v2 8 × 60K Microarray (Agilent Technologies), according to the One-Color Microarray-Based Gene Expression Analysis kit protocol (Version 6.9.1). Raw signal values were thresholded to 1, log2 transformed, normalized to the 75th percentile, and baselined to the median of all samples using GeneSpringGX v.14.9 (Agilent Technologies). To remove unreliable data, all genes from all samples were quality-filtered to include only probes flagged "detected" in at least 100% of all samples in one out of the two genotypes tested. Filtering data by quality-control criteria short-listed 32,655 probes as our complete Data Set, out of a total of 56745 probes present on the microarray. To assess the statistical significance of gene expression changes in *Gjb2*$^{-/-}$ mice versus *Gjb2*$^{loxP/loxP}$ age-matched controls, statistical analysis was performed by

---

[2] https://www.ncbi.nlm.nih.gov/books/NBK1434/.
[3] http://swissvar.expasy.org/cgi-bin/swissvar/result?global_textfield=gjb2&findProteins=search.
[4] http://deafnessvariationdatabase.org/letter/g, then select "*GJB2*".
[5] https://www.ncbi.nlm.nih.gov/books/NBK1434/.
[6] Online Mendelia Inheritance in Men, https://www.omim.org/.
[7] https://www.ncbi.nlm.nih.gov/books/NBK1272/.
[8] https://www.rcsb.org/structure/5NLB.

[9] https://www.infrafrontier.eu/.
[10] https://www.taconic.com/.
[11] http://www.mousephenotype.org/.

using the GeneSpring GX software package (version 14.9, Agilent Technologies). In particular, we used a moderate *t*-test and differentially expressed genes with a p-value ≤ 0.05 were deemed as significant (Supplementary material, Data Set No.1). Genes with deregulated expression changes were screened for gene ontology and pathway enrichment analyses (where Fisher's Exact with FDR multiple test correction p < 0.001, was applied) using specialized bioinformatics tools and databases: Enrichr (http://amp.pharm.mssm.edu/Enrichr), Ingenuity Pathway Analysis (Qiagen) and MetaCore (Thomson Reuters, Toronto, Canada). The subset of DEGs regulated by Nrf2 has been inferred by MetaCore database annotations [25-28].

2.3. GSH release assay

Both cochleae from each P5 mouse pup were quickly dissected in ice-cold Hepes buffered (pH 7.2) Hank's Balanced Salt Solution (HBSS; ThermoFisher, Cat. No. 14025050) and placed onto a 5 mm glass coverslip coated with Cell-Tak (Biocoat, Cat. No. 354240). Coverslips were incubated overnight at 37 °C in DMEM/F12 (ThermoFisher, Cat. No. 11320-074) supplemented with 5% FBS (ThermoFisher, Cat. No. 10270-106) and 100 µg/ml ampicillin (Sigma-Aldrich, Cat. No. A0166). The following day, complete DMEM was removed, cochlear cultures were washed once with serum free DMEM, transferred (with their 5 mm coverslips) into a 96 well plate and allowed to rest for 30 min at 37 °C and 5% CO_2. To perform the GSH release assay, cultures were incubated for 40 min at 37 °C and 5% CO_2 with 120 µL of a solution containing either 1.8 mM Ca^{2+} (HC) or 0 mM Ca^{2+} (LC) and (in mM): 137 NaCl, 5.36 KCl, 0.81 Mm $MgSO_4$, 0.44 KH_2PO_4, 0.18 Na_2HPO_4, 0.1 EGTA, 25 HEPES and 5.55 Glucose, pH 7.3. To quantify the level of released glutathione, 100 µL of supernatant was collected from each well and transferred to a 96 well plate to be used in conjunction with a GSH/GSSG Ratio Detection Assay kit (Fluorometric – Green, ab13881, abcam, Cambridge Science Park, UK) based on a non-fluorescent dye that becomes strongly fluorescent upon binding the released GSH. Fluorescence was measured in a multi-well plate reader (Varioskan Lux, Thermo Fisher Scientific) by exciting samples at 490 nm and detecting fluorescence emission at 520 nm. GSH standard curves were generated by serially-diluted concentrations of GSH and used to convert measurements of fluorescence signals into GSH concentration.

2.4. Measurement of ABRs and DPOAEs

Auditory function was assessed in a sound-attenuating enclosure (ETS-Lindgren SD Test Enclosure, MDL Technologies Limited, Hitchin, U.K.) using an ABR Workstation (Tucker-Davis Technologies, Inc., Alachua, FL, U.S.A.) comprising: Z-Series 3-DSP Bioacoustic System w/ Attenuators and Optic fiber; Medusa 4-Channel Pre-Amp/Digitizer; Medusa 4-Channel Low Imped. Headstage; MF1-M Multi Field Magnetic Speakers – Mono; AEP/OAE Software for RZ6; Experiment Control Workstation. Sound levels were calibrated using a ¼ in. Free Field Measure Calibration Microphone Kit (Model 480C02; PCB).

Mice were anesthetized with intraperitoneal injections of ketamine (70 mg/g for males, 100 mg/g for females) and medetomidine (1 mg/g). The depth of anesthesia was periodically verified by the lack of foot-pinch response. Body temperature was maintained at 37 °C using a heating pad under feedback control. Corneal drying was prevented by application of ophthalmic gel to the eyes of the animals.

For ABR recordings [29], acoustic stimuli consisted of clicks (100 µsec duration) and tone bursts (1 ms rise–fall time with 3 ms plateau) of 4, 8, 16, 24 and 32 kHz were delivered in the free field using a MF1-M speaker. Bioelectrical potentials were collected with gauge 27, 13 mm needle electrodes (Cat. No. S83018-R9, Rochester) inserted subdermally at the vertex (active), ventrolateral to the left ear (reference) and above the tail (ground). Potentials were amplified, filtered (0.3–3 kHz) and averaged over 512 presentations of the same stimulus. Hearing threshold levels were determined offline as the sound pressure level (SPL) at which a Wave II peak, could be visually identified above the noise floor (0.1 µV).

Otoacoustic emissions [30,31] were evoked using a pair of equal intensity primary tones, $f_1 = 14{,}544$ Hz, and $f_2 = 17{,}440$ kHz delivered at intensities ranging from 20 to 80 dB SPL in 10 dB SPL increments. Each primary tone (20.97 ms duration, 47/sec) was emitted by a separate MF1-M speaker, configured for closed field stimulation, and delivered to the mouse ear via a small tube as prescribed by the manufacturer. The cubic distortion product $2f_1 - f_2 = 11{,}648$ kHz, was detected using a small microphone (ER10B+ Low Noise Probe and Microphone, Etymotic Research, IL, U.S.A.) coupled to the ear canal.

After the final ABR test, animals were terminally anesthetized (ketamine, 70 mg/g for males, 100 mg/g for females and medetomidine 1 mg/g), cochleae were quickly removed and samples were fixed with 4% paraformaldehyde in PBS at 4 °C and a pH 7.5. Next, cochleae were decalcified for 3 days in EDTA 10%, incubated for 48 h in sucrose (30%), embedded in OCT, cryosectioned at a thickness of 6 µm (Cryostat SLEE), and processed as described hereafter.

2.5. Immunohistochemistry and confocal imaging

Specimens were included in 3% agarose dissolved in PBS and cut in 100 µm thickness steps using a vibratome (VT 1000 S, Leica Biosystems Nussloch GmbH, Nussloch, Germany). Tissue slices were permeabilized with 0.1% Triton X–100, dissolved in bovine serum albumin (BSA)2% solution. Cx26 was immunolabeled by overnight incubation at 4 °C with a mouse monoclonal anti-Cx26 selective antibody (10 µg/ml, ThermoFisher, Cat. No. 335800). Secondary antibody (10 µg/ml) was Alexa Fluor® 488 goat anti-mouse (IgG, ThermoFisher, Cat. No. A11029), applied at room temperature (22–25 °C). F–Actin was stained by incubation with AlexaFluor 568 phalloidin (1 U/ml, ThermoFisher, Cat. No. A12380), and nuclei were stained with 4′,6–diamidino–2–-phenylindole (DAPI, ThermoFisher, Cat. No. D1306) (1:200).

To quantify hair cell survival, cochleae were quickly dissected from adult mice and tissue samples were fixed with 4% paraformaldehyde. F–Actin was stained by incubation with ActinGreen 488 Ready Probes Reagent (ThermoFisher, Cat. No. R37110).

All samples were mounted onto glass slides with a mounting medium (FluorSaveTM Reagent, Merk, Darmstadt, Germany, Cat. No. 345789) and analyzed using a confocal microscope (TCS SP5, Leica, Wetzlar, Germany) equipped with an oil–immersion objective (40× HCX PL APO 1.25 N.A., Leica).

2.6. Hematoxylin Eosin staining

To quantify SGN survival, cochleae were quickly removed and samples were fixed with 4% paraformaldehyde in PBS at 4 °C and a pH 7.5. Next, cochleae were decalcified for 3 days in 10% EDTA, incubated for 48 h in sucrose (30%), embedded in OCT and cryosectioned at a thickness of 6 µm (Cryostat CM 1950; SLEE, Mainz, Germany). The sections were stained with hematoxylin and eosin (H&E) for the histological assessment of ganglion neuronal cell damage, which is dependent on viable and nonviable stained cells. A standard H&E protocol was followed with a 4–5 min incubation in hematoxylin and 45 s staining in eosin then mounted with Entellan® (Cat. No. 107960, Merck). The cross-sectional area of Rosenthal's canal was measured using NIH Image. Viable neurons with a clear round nucleus and homogeneous cytoplasm were then counted. The SGN density (cells per square millimeters) was calculated using NIH ImageJ 1.43u (Image Processing and Analysis in Java).

2.7. TUNEL Assay

TUNEL (APO-BrdU™ TUNEL Assay Kit, Cat. No. A23210, ThermoFisher) was used to detect DNA fragmentation in the nuclei of apoptotic cells in the organ of Corti and SGNs. The assay was performed

according to manufacturer's instructions on cochlear cryosections from $Gjb2^{loxP/loxP}$ and $Gjb2^{+/-}$ mice at 6 months of age (MoA). Cochleae were quickly removed, and the samples were fixed with 4% paraformaldehyde in PBS at 4 °C and a pH 7.5. Next, cochleae were decalcified for 3 days in 10% EDTA, incubated for 48 h in sucrose (30%), embedded in OCT and cryosectioned at a thickness of 6 μm (Cryostat CM 1950; SLEE). All procedures were performed under dim light. Briefly, the specimens were incubated 3 h in ice-cold 70% (v/v) ethanol and then incubated overnight at room temperature in freshly prepared DNA-labeling solution. The specimens were rinsed twice in the rinse buffer and then stained with Anti-BrdU mouse monoclonal antibody PRB-1, Alexa Fluor 488 conjugate for 1 h at room temperature. The slices were further stained with PI (Propidium Iodide, 1:100) for 20 min at room temperature. After rinsing in PBS, specimens were coverslipped with an antifade medium (Pro Long Gold, Cat. No. P36930, ThermoFisher). Cells with intense yellow-labeled nuclei (red plus green) were identified as apoptotic cells.

2.8. Detection of ROS formation and lipid peroxidation

To assess oxidative damage level, we used dihydroethidium (DHE) staining and 4-hydroxy-2-nonenal (4-HNE) immunostaining. DHE and 4-HNE (a by-product of lipid peroxidation) provided indications on production of the toxic superoxide anion and oxidative degradation of lipids generated by the effect of free radicals, respectively.

2.8.1. DHE assay

DHE is a lipophilic cell-permeable dye that is rapidly oxidized to ethidium in the presence of free radical superoxide. In theory, the produced ethidium is fixed by intercalation into nDNA; it gives an indication of oxidant stress within cells undergoing investigation [32-34]. The cochlear specimens were incubated with 1 mM DHE (Cat. No. D23107, ThermoFisher) in PBS for 30 min at 37 °C and then coverslipped with the antifade medium. The staining was imaged by two-photon excitation (792 nm, 140 fs, 80 MHz) performed by an ultrafast tunable mode-locked titanium: sapphire laser (Chameleon; Coherent) coupled to a multiphoton microscope (A1R MP+, Nikon). Images were taken at 20× (Plan Apo objective, 0.75 N.A., Nikon).

2.8.2. 4-HNE assay

Specimens were incubated with a blocking solution (1% BSA, 0.5% Triton X-100 and 10% normal goat serum in PBS 0.1 M), thereafter slices were incubated overnight at 4 °C with a solution containing rabbit polyclonal anti4-HNE primary antibody (rabbit Anti4-HNE antiserum, Cat#HNE11-S, Alpha Diagnostic Int., SanAntonio, USA) diluted 1:100 in PBS. All specimens were incubated at room temperature for 2 h in label-conjugated goat anti-rabbit secondary antibody (Alexa Fluor 488, IgG, Cat. No. A32731, ThermoFisher) diluted 1:400 in 0.1 M PBS and additionally stained with DAPI (1:500 in 0.1 M PBS). Images were obtained with a confocal laser scanning system (Ti-E, Confocal Head A1 MP, Nikon, Japan). equipped with a 20x Plan Apo objective (0.75 N.A., Nikon). For each immunostaining procedure, control experiments (negative controls not shown) were performed by omitting the primary antibody during processing of tissue randomly selected across experimental groups. Tissues from all groups were always processed together during the procedures to limit variability related to antibody penetration, incubation time, post-sectioning age, and condition of tissue.

2.9. Measurement of endogenous antioxidant defenses

2.9.1. Western Immunoblot

Total proteins were extracted from cochleae of $Gjb2^{+/-}$ and $Gjb2^{loxP/loxP}$ animals at 2, 6 and 12 MoA. To extract sufficient protein, cochleae were dissected, collected on ice and stored at −80 °C. Cochleae were pooled (n = 8 for each genotype at each time point), homogenized by using ice cold RIPA buffer (Pierce, Rockford, IL, USA,

Table 1

Transcriptomic and functional analysis of the P5 cochlea from $Gjb2^{-/-}$ mice versus $Gjb2^{loxP/loxP}$ age-matched controls. The table lists the most significant signaling cascades and ranks related genes for *Metabolic Process* (GO:0008152) that were statistically altered (moderate *t*-test, p-value ≤ 0.05) in $Gjb2^{-/-}$ mice and under transcriptional control of Nrf2. KO = $Gjb2^{-/-}$; WT = $Gjb2^{loxP/loxP}$. For more details, please refer to Supplementary material, Data Set No. 3.

Signaling pathway	GeneSymbol	p-value	Fold change ([KO] / [WT])
Oxidative metabolism and antioxidant defense systems	Rb1cc1	0.048	1.510
	Prkce	0.041	1.578
	Mef2c	0.035	1.693
	Ep300	0.026	1.732
	Atr	0.034	1.799
	Nfatc3	0.023	1.915
	Pten	0.010	2.053
	Acox3	0.010	2.149
	Nox4	0.018	2.783
	Smad1	0.003	2.854
Glutathione metabolism	Gpx3	0.005	− 2.202
	Gss	0.041	− 1.816
	Shmt2	0.048	− 1.570
	Gstt2	0.035	1.747
	Ahcyl2	0.047	2.116
MAPK Signaling Pathway	Tgfb1	0.005	− 2.497
	Map4k4	0.023	− 1.658
	Snail1	0.024	− 1.656
	Map3k11	0.047	− 1.509
	Map3k1	0.036	1.609
	Pdgfb	0.042	1.624
	Mef2c	0.035	1.693
	Mknk1	0.026	1.702
	Map3k2	0.041	1.786
	Mapk6	0.044	1.799
	Map3k12	0.009	1.854
	Rasa2	0.013	2.131
	Nf1	0.040	2.676
	Ikbkb	0.011	2.810
	Mapk1	0.006	3.077

Cat. No. PI89900, 50 mM Tris, 150 mM NaCl, 1 mM EDTA, 1% DOC, 1% Triton X-100, 0.1% SDS and 1× protease, Cat. No. P8340 phosphatase-1, Cat. No. P2850 and phosphatase-2 inhibitor cocktails, Cat. No P5726 [Sigma-Aldrich]). The lysate was sonicated 3 times at 10 Hz (Hielscher, Ultrasound Technology UP50H/UP100H), centrifuged (13,000 rpm, 15 min, 4 °C), and a 5-μL aliquot of the supernatant was assayed to determine the protein concentration (microBCA kit, Cat. No. 23235, Pierce, Rockford, IL, USA). Reducing sample buffer was added to the supernatant, and samples were heated to 95 °C for 5 min.

Samples used for GSH analyses were processed under non reducing conditions to identify multiple bands at variable molecular weights in order to detect all glutathionylated proteins [32]. Protein lysates (70 μg) were loaded onto 4–15% Tris-glycine polyacrylamide gels for electrophoretic separation. Colorburst™ Electrophoresis markers (Sigma) were used as molecular mass standards. Proteins were then transferred onto nitrocellulose membranes at 100 V for 2 h at 4 °C in transfer buffer containing 25 mM Tris (Cat. No. T4661, Sigma-Aldrich), 192 mM glycine (Cat. No. G8898, Sigma-Aldrich), 0.1% SDS (Sodium Dodecyl Sulfate, Cat. No. L3771, Sigma-Aldrich), and 20% methanol (Cat. No. 322415, Sigma-Aldrich). Membranes were incubated for 1 h with blocking buffer (5% skim milk [Cat. No. #1706404, Bio-Rad Laboratories, Hercules, CA, USA] in TBST [Tris Buffered Saline, Cat. No. T5912, Sigma-Aldrich and 0.1% Tween 20, Cat. No. P1379, Sigma-Aldrich]), and then incubated overnight at 4 °C with the following primary antibodies: anti-Nrf2 (mouse monoclonal, 1:1000; Cat. No. 89443 Abcam, Cambridge, MA, USA); anti HO-1 (rabbit polyclonal, 1:1000; Cat. No. ADI-SPA-896D StressGen Biotechnology, Victoria, Canada); anti-GSH (mouse monoclonal, 1:1000; Cat. No 19534, Abcam). After three 10-min rinses in TBST, membranes were incubated
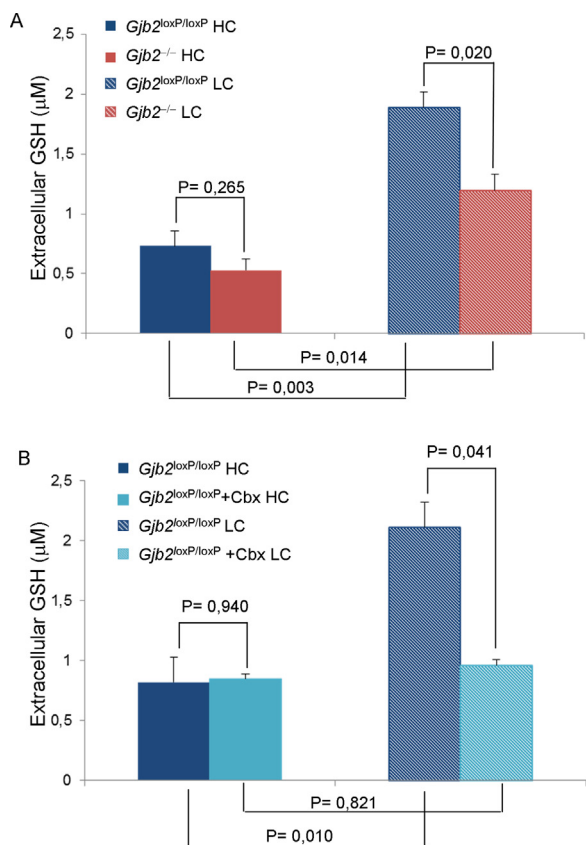
Fig. 1. GSH release assay in cochlear organotypic cultures from P5 $Gjb2^{-/-}$ mice. A: Release of GSH during incubation of $Gjb2^{loxP/loxP}$ and $Gjb2^{-/-}$ cochlear cultures exposed to high Ca^{2+} (1.8 mM, HC) or low Ca^{2+} (0 mM, LC) solutions. B: Inhibition of GSH release by carbenoxolone (Cbx, 100 µM) in $Gjb2^{loxP/loxP}$ cochleae. Data are mean ± s.e.m. for m = 6 cochleae from n = 3 mice in each condition; p-values were determined by two-tailed t-test.

for 1 h at RT HRP-conjugated mouse or rabbit secondary antibodies (1:2500; Cat. No. 70765, Cell Signaling, Danvers, MA, USA). Equal protein loading among individual lanes was confirmed by reprobing the membranes with an anti-GAPDH mouse monoclonal antibody (1:10,000; Cat. No. 9485, Abcam). The membranes were then washed,

and the bands were visualized with an enhanced chemiluminescence detection kit (Cat. No. RPN2232, GE Healthcare, Cardif, UK). Protein expression was evaluated and documented by using UVItec, Cambridge Alliance. Values are expressed as Nrf2 and HO-1/GAPDH ratio. As regard GSH, values are expressed as optical density of multiple bands at all molecular weights.

2.9.2. Immunofluorescence analyses

Specimens were incubated with a blocking solution (1%BSA [Bovine Serum Albumin, Cat. No. A9647, Sigma-Aldrich], 0.5% Triton X-100 [Cat. No. T8787, Sigma-Aldrich] and 10% normal goat serum [Cat. No. S26-M, Sigma-Aldrich] in PBS 0.1 M), thereafter slices were incubated overnight at 4 °C with a solution containing anti-GSH (Cat. No. 19534, Abcam, Cambridge, MA, USA) or anti-HO-1 (Cat. No. ADI-SPA-896D Stressgen, Victoria, Canada) and Nrf2 (Cat. No. 89443, Abcam) primary antibodies diluted 1:100 in PBS. After washing in PBS, samples were incubated at room temperature for 2 h in labeled conjugated goat anti-rabbit (HO-1) (Alexa Fuor 488 Cat. No. A-11034, ThermoFischer, Waltham, MA, USA.) or donkey anti-mouse (GSH, Nrf2) secondary antibody (Alexa Fluor 488, Cat. No. A- 21202; or Alexa Fluor 546, IgG, Cat. No. A 10036, ThermoFischer) diluted 1:400 in 0.1 M PBS and stained with DAPI stained (1:500 in 0.1 M PBS).

2.10. Transfer assay for the non-metabolizable D-glucose analogue 2-NBDG

2-(N-(7-nitrobenz-2-oxa-1,3-dia-zol-4-yl)amino)-2-deoxyglucose (2-NBDG, ThermoFisher Cat. No. N13195, MW = 342.3) is a fluorescent glucose analogue that has been used to monitor glucose uptake in live cells [35] and in the sensory epithelium of the cochlea [36]. Following *in vivo* delivery as previously described [36], cochleae were rapidly dissected in HBSS, supplemented with Cbx (100 µM) to limit dye escape via open connexin hemichannels. The freshly explanted tissue was then transferred on the motorized stage (Proscan III, Prior, Cambridge, UK) of a laser scanning multiphoton confocal microscope (Bergamo 2, Thorlabs, Ely, UK) equipped with water immersion objective (25×, N.A. 1.05, XLPLN25XWMP2, Olympus, Tokyo, Japan) and coupled to a femtosecond pulsed laser source (Camelion Ultra II, 680–1080 nm, 3.5 W, Coherent). 2-NBDG fluorescence was excited at λ = 890 nm and detected with a Semrock 525/40 nm band bandpass filter (FF02-525/40-25). Control experiments were performed by replacing 2-NBDG with D-glucose (Sigma-Aldrich, Cat. No. D9434) in the injection buffer. Images were stored in the computer hard disk for offline analysis. The
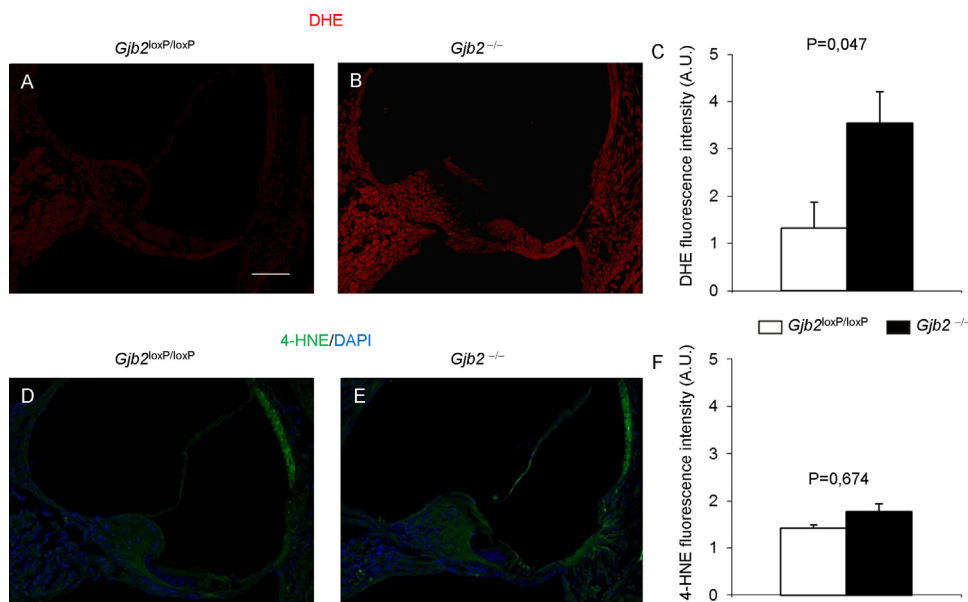

Fig. 2. DHE and 4-HNE staining in cochlear organotypic cultures from P5 $Gjb2^{-/-}$ mice. A, B: Representative DHE staining in confocal fluorescence images of midmodiolar transversal cryosections from $Gjb2^{loxP/loxP}$ and $Gjb2^{-/-}$ cochlear samples. D, E: Corresponding 4-HNE expression. Scale bar: 100 µm. C, F: Fluorescence emission intensity (A.U., arbitrary units) for DHE (C) and 4-HNE (F). Data are mean ± s.e.m. for m = 3 cochleae from n = 3 mice in each condition; p-values were determined by two-tailed t-test.
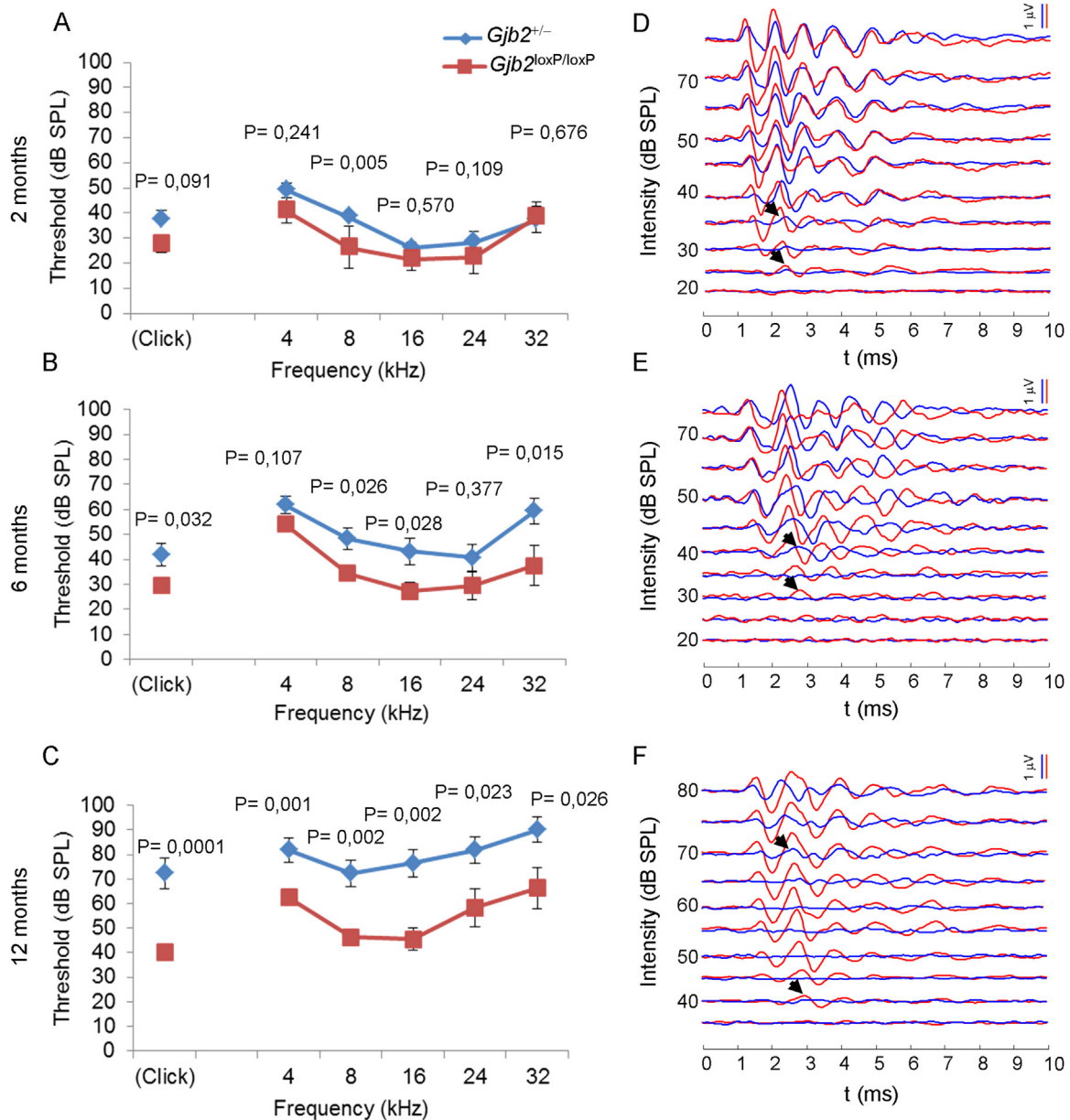
Fig. 3. Auditory threshold evaluation by ABRs at 2, 6 and 12 MoA in $Gjb2^{+/-}$ mice. A–C: *In vivo* electrophysiological recordings (averaged threshold values ± s.e.m.) showing click responses and tone burst responses at 4, 8, 16, 24 and 32 kHz in $Gjb2^{loxP/loxP}$ (red squares) and $Gjb2^{+/-}$ mice (blue diamonds) at 2 (A), 6 (B) and 12 (C) MoA. The number of mice used was n = 10 for each condition; p-values were determined by two-tailed *t*-test. D–F: Representative recordings of ABR evoked by clicks in $Gjb2^{loxP/loxP}$ (red) and $Gjb2^{+/-}$ mice (blue) at 2 (D), 6 (E) and 12 (F) MoA; arrows indicate threshold level.

fluorescent intensity of each area of interest was quantified with ImageJ (version 1.51 s) and statistics were computed with a spread sheet (*Microsoft Office Excel* 2017, Version 1.30).

2.11. Analyses of human cohorts

2.11.1. Phenotypes and genotypes

An overall number of 4091 subjects aged more than 18 years with hearing phenotype were included in **Analysis 1**. This cohort includes also 2366 individuals used in the ARHL case-control study (**Analysis 2:** 1076 presbycusis patients and 1290 healthy matched controls). Among them, 3032 subjects come from different isolated cohorts located in Europe, Caucasus and Central Asia as previously described [37], while 1059 additional subjects belong to a Belgian cohort [38]. For **Analysis 1**, audiometric data collection and phenotypic criteria have been previously detailed [39]. For **Analysis 2**, the pure-tone average of air

conduction at high frequencies (4,8 kHz) (henceforth referred to as PTAH) was computed and used to define case-control status with respect to presbycusis. In particular, subjects aged 50 or older with PTAH value greater than or equal to 40 dB were considered as ARHL-cases, while subjects aged 50 or older with PTAH value lower than or equal to 25 dB were regarded as healthy controls [40]. ARHL-cases were conveniently selected excluding those individuals exposed to noise or with a genetic history of hearing loss.

Genotype and phenotype data were obtained as previously described [41,42,40]. Genotypes were then imputed as follows: the phasing step was carried out using SHAPEIT2 [43], and IMPUTE2 [44] was used to impute data to the 1000 Genomes Phase 1 v3 reference set [45]. After the imputation phase, SNPs with info score (imputation quality) < 0.4 and MAF < 0.01 were excluded.
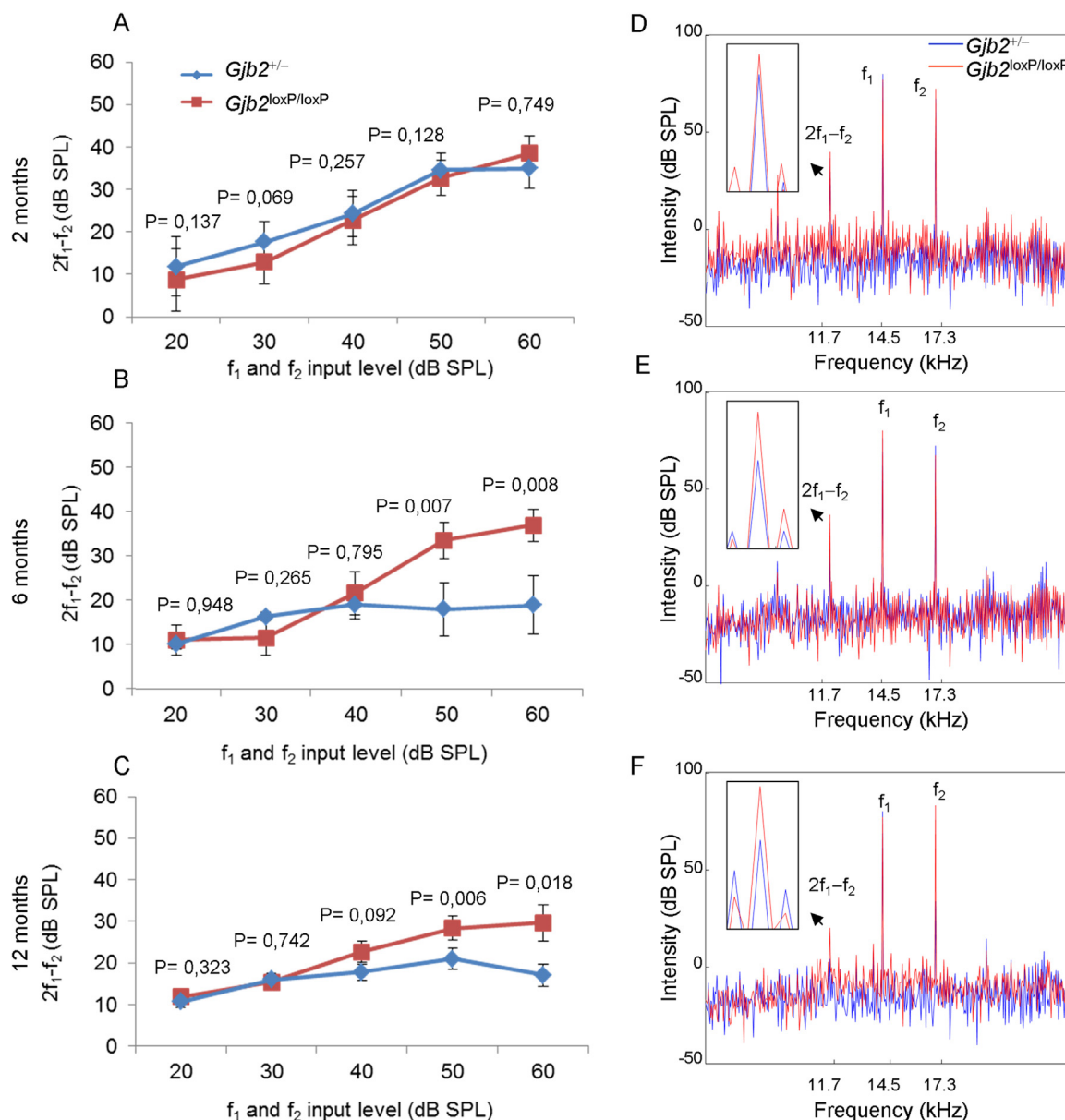
Fig. 4. Measurement of DPOAEs at 2, 6 and 12 MoA in *Gjb2*$^{+/-}$ mice. A-C: DPOAE recordings (mean $\pm$ s.e.m., see Section 2.4) in *Gjb2*$^{\text{loxP/loxP}}$ and *Gjb2*$^{+/-}$ mice at 2 (A), 6 (B) and 12 (C) MoA. The number of mice used was n = 10 for each condition; p-values were determined by two-tailed *t*-test. D–F: Representative DPOAE spectra in *Gjb2*$^{\text{loxP/loxP}}$ mice (red) and *Gjb2*$^{+/-}$ mice (blue) at 2 (D), 6 (E) and 12 (F) MoA; insets show a magnified view of the spectrum in the region of the $2f_1 - f_2$ cubic distortion product.

2.11.2. Association analysis and meta-analysis

On each cohort, genome-wide association studies (GWAS) were carried out for the normal hearing function (hearing threshold at 250 Hz, 500 Hz, 1 kHz, 2 kHz, 4 kHz and 8 kHz) and ARHL case-control studies as described in Vuckovic et al. [39]. Methodology used were GRAMMAR-Gamma method on genotyped SNPs and MixABEL on imputed ones, as available in the GenABEL suite. In particular, p-values for the genotype-phenotype association shown in Table 5 were determined using the Wald Chi-Squared test, as implemented in GenABEL package [46]. Results from single cohorts were then pooled together using METAL software [47], performing a fixed-effects meta-analysis with inverse variance weights. Starting from a list of 29 human genes orthologous to the murine ones defined in Table 1, a candidate gene approach on the results from the GWAS meta-analysis was performed. As a first step, for every analyzed trait, all polymorphisms with p-value above nominal significance threshold were filtered out. Bonferroni correction was then applied on the p-values of the remaining polymorphisms.

2.12. Statistical analysis

For normally distributed data, statistical comparisons of means data were made by Student's two-tailed *t*-test [48] using a worksheet (*Microsoft Office Excel* 2017, Version 1.30), whereas ANOVA and post-hoc comparison by Tuckey's test [49] were used to analyze the differences among group means using *Statistica* (version 6.0, Statsoft Inc.). The same software was also used to perform the Mann-Whitney *U* test [50] on data that did not require the assumption of normal distribution. Mean values are quoted $\pm$ standard error of the mean (s.e.m.) where p-values < 0.05 indicate statistical significance.

2.13. Study approval

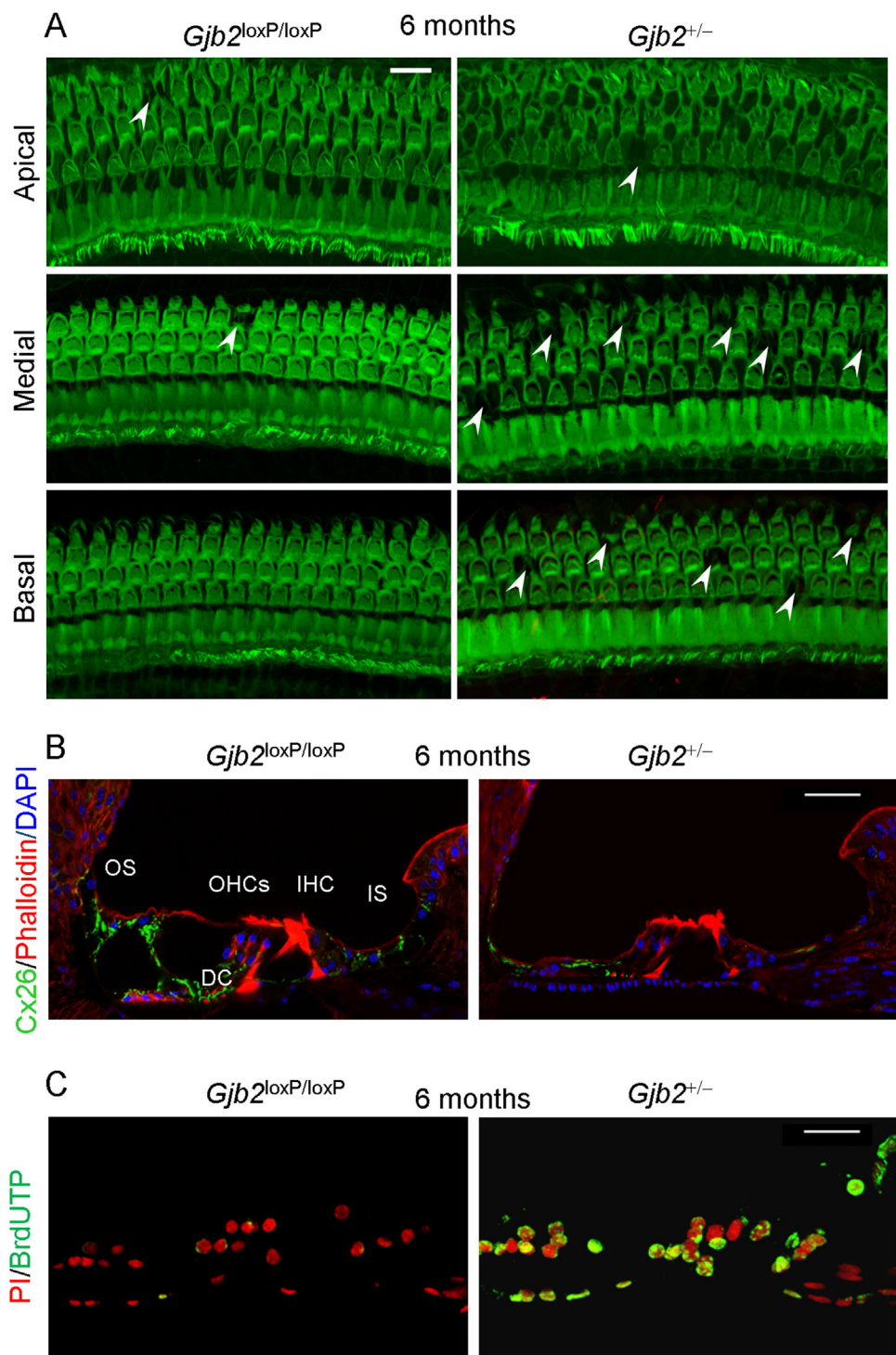The work described has been carried out in accordance with The

Fig. 5. Gross morphology and apoptosis in the organ of Corti at 6 MoA in *Gjb2*^{+/−} mice. A: Representative horizontal sections, orthogonal to the modiolus, of cochleae from *Gjb2*[loxP/loxP] and *Gjb2*^{+/−} mice; images from apical, medial and basal turns were obtained by maximal intensity back–projection of 15 confocal optical sections from a 0.8 μm step though–focus sequence (z–stack); actin filaments were stained with ActinGreen 488 ReadyProbes (green); arrowheads indicate missing outer hair cells; scale bar: 50 μm. For data quantification, see Table 2. B: Maximal projection rendering of two consecutive confocal optical sections taken at 0.6 μm intervals; immunofluorescence staining shows Cx26 expression (green) in Deiters cells (DC), inner sulcus (IS), outer sulcus (OS); nuclei were stained with DAPI (blue), and actin filaments with red conjugated phalloidin; OHCs, outer hair cells; IHC, inner hair cell; gamma filters were applied to both red (g = 0.65) and blue (g = 0.75) channels; scale bar: 20 μm. C: Confocal images of midmodiolar transversal cryosections showing the organ of Corti of *Gjb2*[oxP/loxP] and *Gjb2*^{+/−} mice stained with propidium iodide (red) and BrdUTP (green); for data quantification, see Table 3.

Code of Ethics of the World Medical Association (Declaration of Helsinki) for experiments involving humans. Informed consent was obtained for experimentation with human subjects and the privacy rights of human subjects was always be observed.

All animal procedures, including care and handling, were conducted in accordance with the protocol approved by the Italian Ministry of Health (Authorization n. 1005/2016-PR, date 21/10/2016, DGSAF Prot. No. 002451-P-25/10/2016), in compliance with the ARRIVE guidelines and the EU Directive 2010/63/EU for animal experiments.

3. Results

3.1. Lack of Cx26 contributes to a diminished antioxidant defense system in the developing cochlea of Gjb2^{−/−} mice

As mentioned in the Introduction, *Gjb2*^{−/−} mice fail to acquire hearing [16,17]. Cx26 immunoreactivity is absent in the epithelial gap junction system of these mice, whereas Cx30 expression is developmentally delayed, such that immunoreactivity for both Cx26 and Cx30 is negligible up to postnatal day 9 (P9, where P0 is date of birth) [16]. To further characterize this mouse strain, we performed an initial set of experiments using a oligonucleotide microarray platform.

Table 2

Percentage of hair cell survival in the apical, middle and basal turn of cochleae from $Gjb2^{+/-}$ and $Gjb2^{loxP/loxP}$ mice at 6 MoA (n = 4 mice of each genotype). Shown are mean percent values, rounded to nearest integer, with standard deviation (in round brackets) and p-values (in square brackets) of $Gjb2^{+/-}$ samples relative to $Gjb2^{loxP/loxP}$ controls determined by the Mann-Whitney U test.

Organ of Corti	Outer hair cells survival (%)		Inner hair cells survival (%)	
	$Gjb2^{loxP/loxP}$	$Gjb2^{+/-}$	$Gjb2^{loxP/loxP}$	$Gjb2^{+/-}$
Apical turn	95 (3)	87 (5) [p = 0.057]	100 (0)	98 (4) [p = 0.41]
Middle turn	96 (2)	89 (1) [p = 0.0015]	97 (4)	98 (4) [p = 0.904]
Basal turn	99 (1)	86 (8) [p = 0.028]	100 (0)	96 (2) [p = 0.685]

Table 3

Percentage of apoptotic cells in the organ of Corti and spiral ganglion of cochlear apical, middle and basal turns from $Gjb2^{+/-}$ mice and $Gjb2^{loxP/loxP}$ controls at 6 MoA (m = 9 cryosections from n = 3 mice of each genotype). Shown are mean values computed over an area of $100\,\mu m \times 100\,\mu m$, with standard deviation (in round brackets) and p-values (in square brackets) of $Gjb2^{+/-}$ relative to $Gjb2^{loxP/loxP}$ determined by the Mann-Whitney U test.

	Apoptotic cells (%)	
	$Gjb2^{loxP/loxP}$	$Gjb2^{+/-}$
Organ of Corti		
Apical turn	8.3 (5.85)	47.75 (6.18) [p = 0.0002]
Middle turn	6.2 (3.9)	63.01 (19.9) [p = 0.0009]
Basal turn	2.94 (2.07)	61.30 (19.3) [p = 0.002]
SGNs		
Apical turn	3.75 (2.01)	23.65 (6.82) [p = 0.002]
Middle turn	1.22 (1.73)	20.10 (4.85) [p = 0.001]
Basal turn	0.64 (1.28)	20.48 (1.11) [p = 0.0001]

Specifically, we compared expression profiles of mRNAs in cochlear tissue from $Gjb2^{-/-}$ pups at P5, taking age-matched $Gjb2^{loxP/loxP}$ mice as controls. Our analysis revealed a total of 1733 genes (1942 probes out of a total of 32655 probes that did pass quality control criteria) showing deregulated expression changes in cochlear samples from $Gjb2^{-/-}$ mice *vs.* $Gjb2^{loxP/loxP}$ mice (Supplementary material, Data Set No.1; we note in passing that two connexin genes, *GJA1* (Cx43) and *GJA3* (Cx46) are upregulated in this Data Set).

According to the Gene Ontology (GO) analysis, deregulated genes in $Gjb2^{-/-}$ samples were mainly involved in *metabolic process* (GO:0008152, 473 genes, p-value = 4.00×10^{-7}), *cellular process* (GO:0009987, 644 genes, p-value = 2.35×10^{-6}), and *response to stimulus* (GO:0050896, 147 genes, p-value = 9.92×10^{-7}) (Supplementary material, Data Set No.2 – **Panel a**). To focus on the most significant signaling cascades and to investigate their role in the context of pathways, we restricted the analysis to deregulated genes associated with *metabolic process* and *cellular process*. We determined that the majority of these deregulated genes in $Gjb2^{-/-}$ samples were specifically involved in the MAPK signaling cascade (*Map3k2, Mef2c, Tgfb1, Map3k1, Pdgfb, Ikbkb, Mknk1, Rasa2, Nf1, Mapk1, Mapk6, Map3k11, Map3k12, Map4k4, Snail1*), oxidative metabolism and antioxidant defense systems (*Nox4, Rb1cc1, Mef2c, Ep300, Nfatc3, Prkce, Pten, Smad1, Acox3, Atr*), as well as glutathione metabolism (*Ahcyl2, Gpx3, Shmt2, Gss, Gstt2*) (Supplementary material, Data Set No.2 – **Panel b**).

Interestingly, several of these genes are under transcriptional control of Nrf2 (Table 1 and Supplementary material, Data Set No. 3), supporting a key role for this transcription factor both in the control of detoxifying and antioxidant defense processes and in the regulation of glutathione metabolism [20-22]. Glutathione is a critically important
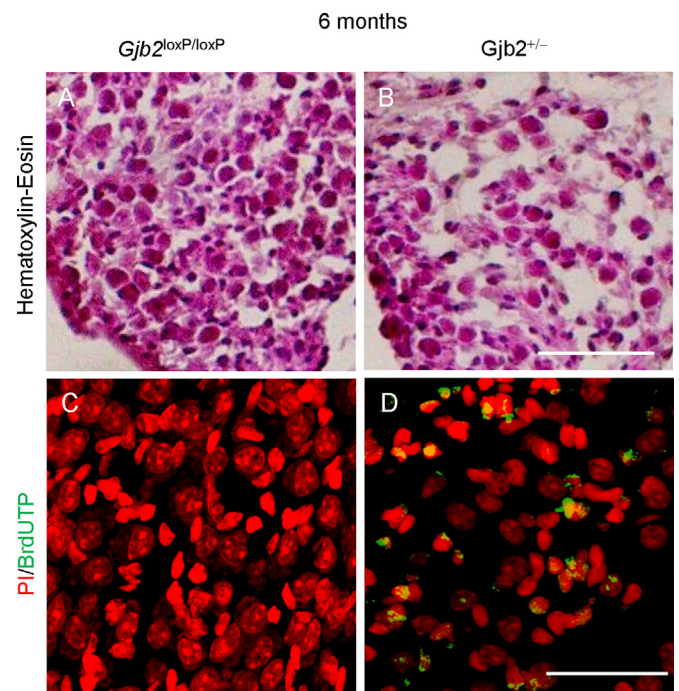
6 months
$Gjb2^{loxP/loxP}$ $Gjb2^{+/-}$

Fig. 6. Gross morphology and apoptosis of SGNs at 6 MoA in $Gjb2^{+/-}$ mice. A, B: Representative SGN Hematoxylin-Eosin staining in $Gjb2^{loxP/loxP}$ (A) and $Gjb2^{+/-}$ samples (B). C, D: Confocal images of midmodiolar transversal cryosections showing spiral ganglion neurons of $Gjb2^{loxP/loxP}$ (C) and $Gjb2^{+/-}$ mice (D) stained with propidium iodide (red) and BrdUTP (green); scale bar: 50 μm. For data quantification, see Table 3.

Table 4

Total number of SGNs in m = 9 cryosections from n = 3 mice of each genotype stained with hematoxylin & eosin. Shown are mean number of cells/mm² with standard deviation (round brackets) and p-values of $Gjb2^{+/-}$ relative to $Gjb2^{loxP/loxP}$ (paired *t*-test, square brackets).

SGNs	6 months	
	$Gjb2^{loxP/loxP}$	$Gjb2^{+/-}$
Apical turn	2606 (259)	1818 (278) [p = 0.0008]
Middle turn	2728 (250)	1910 (499) [p = 0.003]
Basal turn	2788 (277)	1730 (169) [p = 0.0005]

tripeptide thiol (γ-glutamyl cysteinyl glycine) that is found either in the reduced sulfhydryl form (GSH) or in the glutathione disulfide (GSSG) oxidized form. Reactive oxygen species (ROS), superoxide anion ($O2^{\cdot-}$), hydroxyl radical (.OH), hydrogen peroxide (H_2O_2) and hydroperoxides (R–OOH), as well as xenobiotics and other organic radicals, are neutralized by GSH through a concerted cascade of detoxification mechanisms involving GPX, GST, GR and GST. In particular, GPX catalyzes the reaction of GSH with H_2O_2, yielding GSSG and water; RG then reduce GSSG to GSH, completing the cycle [51,52].

In the brain, astrocytes contribute to neuronal detoxification from ROS by releasing GSH [53] through plasma membrane hemichannels formed by Cx43 [54]. Nonsensory cells of the inner ear bear important similarities to glial cells. In particular, all cochlear supporting cells express the glial fibrillary acidic protein (GFAP) marker early after birth, in a gradient decreasing in intensity from the base to the apex of the cochlea [55]. In addition, functional Cx26 hemichannels are present on the surface of cochlear non-sensory cells [15,56-58], and Cx26 hemichannels reconstituted in liposomes are permeable to GSH [59]. Therefore, we reasoned that cochlear nonsensory cells could potentially participate in detoxification from ROS by releasing GSH through Cx26 hemichannels, and this ability might be impaired in the developing
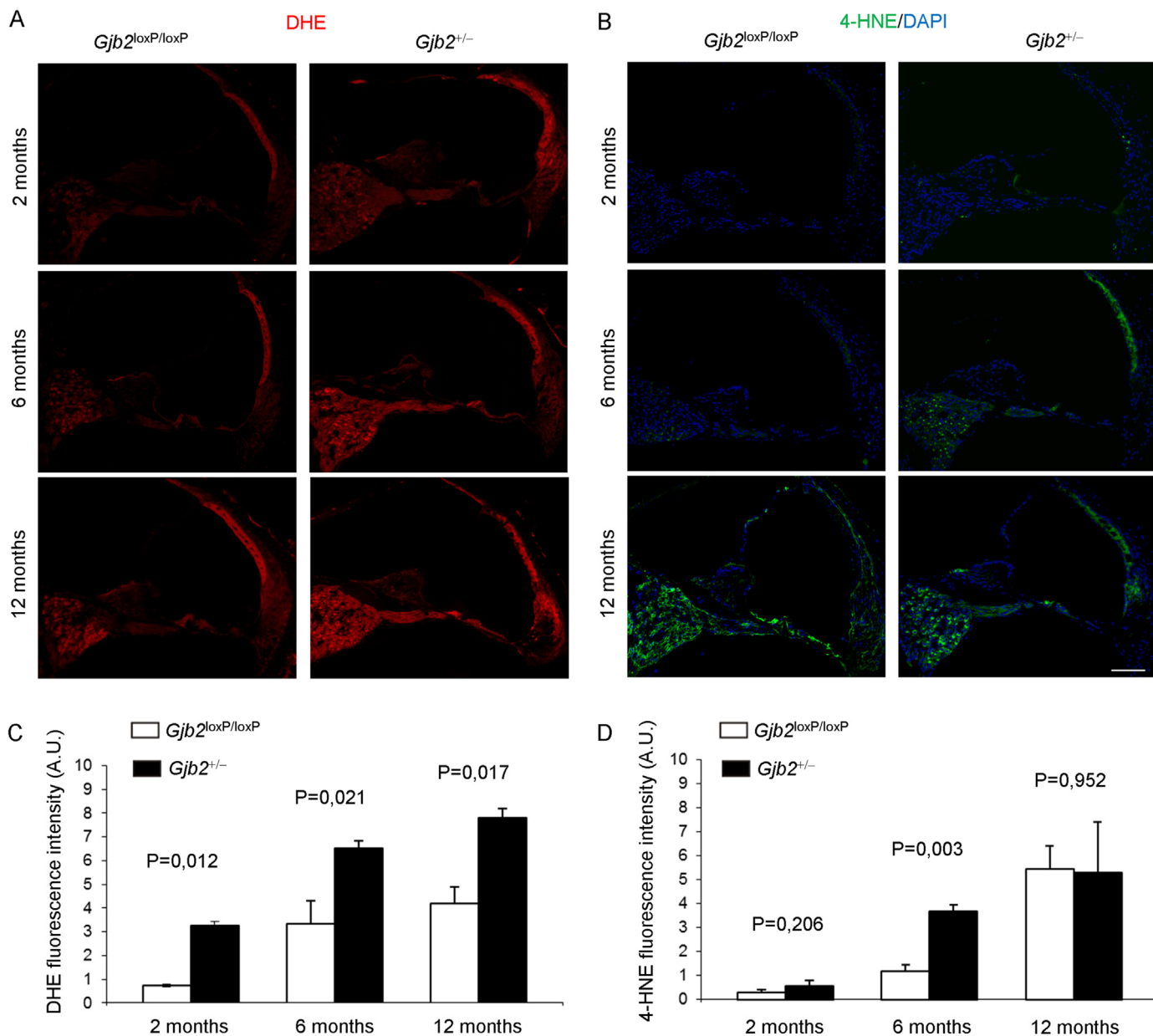
Fig. 7. Exacerbated age-induced oxidative stress in the cochlea of *Gjb2*$^{+/-}$ mice. A: Representative confocal fluorescence images of DHE staining in mid-modiolar transversal cryosections of *Gjb2*$^{loxP/loxP}$ and *Gjb2*$^{+/-}$ samples at 2, 6 and 12 MoA B: Corresponding 4-HNE expression, showing lipid peroxidation in *Gjb2*$^{2loxP/loxP}$ and *Gjb2*$^{+/-}$ samples at 2, 6 and 12 MoA; Scale bar: 100 μm. C, D: Histograms (mean ± s.e.m.) represent fluorescence intensity values (A.U., arbitrary units). P-values were determined by two-tailed *t*-test; n = 3 mice were used for each condition.

cochlea of *Gjb2*$^{-/-}$ mice.

To assay GSH release, we used a sensitive fluorescence-based assay in cochlear organotypic cultures from P5 mice (see Section 2) while lowering the extracellular concentration of Ca^{2+} ([Ca^{2+}]$_e$) from 1.8 mM (HC) to 0 mM (LC), which increases the open probability of most hemichannels [60,61]. As shown in Fig. 1, the amount of GSH released in LC conditions was significantly lower in *Gjb2*$^{-/-}$ cultures than in *Gjb2*$^{loxP/loxP}$ controls (Fig. 1A). GSH release was blocked by carbenoxolone (Cbx, 100 μM), the best known and widely used, albeit non-specific, inhibitor of connexin channels [62] (Fig. 1B).

Based on these results, we predicted that the combined effect of deregulated genes in cochlear samples (Table 1 and Supplementary material, Data Set No. 3) and reduced GSH release (Fig. 1) should lead to increased levels of oxidative stress in the cochlea of *Gjb2*$^{-/-}$ pups. To test this hypothesis, we performed staining of P5 cochlear mid-modiolar transversal section with dihydroethidium (DHE), a lipophilic

cell-permeable dye that is rapidly oxidized to ethidium in the presence of superoxide free radical [63] (Fig. 2A–B). Quantitative image analysis performed over triplicate replicas for each genotype revealed a significantly higher DHE signal in cochlear duct structures obtained from P5 *Gjb2*$^{-/-}$ mice compared to age-matched *Gjb2*$^{loxP/loxP}$ controls (p-value = 0.047, two-tailed *t*-test; Fig. 2C). We also performed immunostaining of 4-hydroxy-2-nonenal (4-HNE), a lipid peroxydation product [64] (Fig. 2D–E), but did not detect significant differences for this marker at this early stage of development (Fig. 2F). A statistically significant increase in the intracellular level of ROS was reported also in the cochlea of deaf *Gjb6*^{tm1Kwi}/*Gjb6*^{tm1Kwi} mice [36] (EM:00323; MGI:2447863),[12] in which Cx30 is deleted globally [65] and cochlear Cx26 is reduced to ~ 10% compared to wild type controls [9,66].

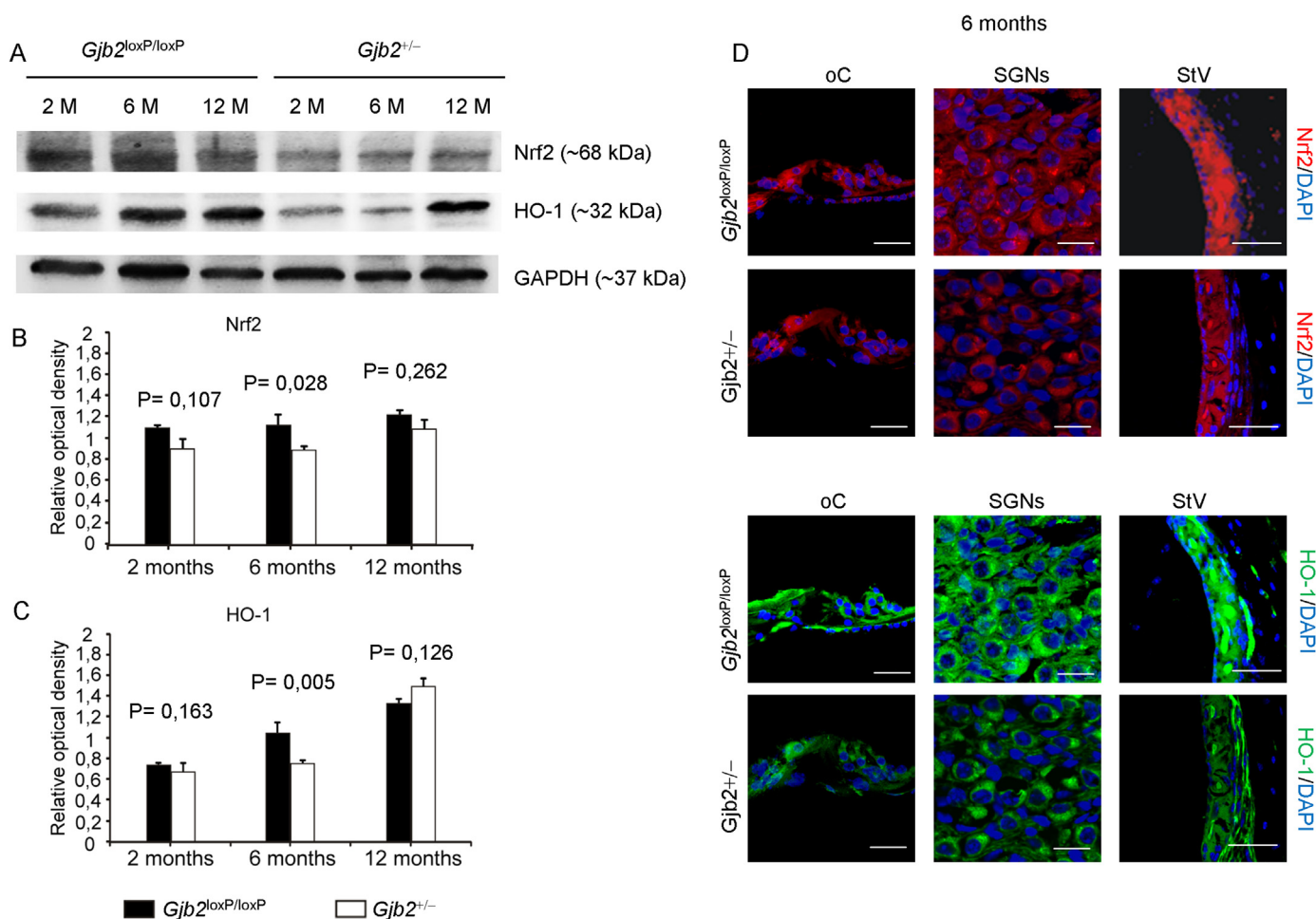[12] Also known as: *Cx30*$^{-/-}$ or *Cx30*-LacZ.

Fig. 8. Decreased levels of endogenous antioxidant defenses in the cochlea of *Gjb2*$^{+/-}$ mice. A: Western blot analysis of Nrf2 and HO-1 expression in *Gjb2*$^{loxP/loxP}$ and *Gjb2*$^{+/-}$ cochleae (n = 8 for each condition) at 2, 6 and 12 months of age (M). B, C: Histograms (mean ± s.e.m.) represent optical density values normalized to GAPDH. Experiments were performed in triplicate and p-values were determined by two-tailed *t*-test. D: Immunofluorescence analysis of Nrf2 (upper panels, red fluorescence) and HO-1 expression (lower panels, green fluorescence) in the organ of Corti (oC), spiral ganglion neurons (SGNs) and *stria vascularis* (StV) at 6 months (M). Scale bars: oC, 20 μm; SGNs, 15 μm; StV, 50 μm.

Therefore, these results strongly suggest that lack of Cx26 in the epithelial gap junction network contributes to a diminished antioxidant defense system in the developing cochlea of *Gjb2*$^{-/-}$ mice. They provide also a putative mechanistic interpretation for the previously reported increase of cell death in the cochlear sensory epithelium of *Gjb2*$^{-/-}$ mice, which leads to complete loss of outer hair cells (OHCs) in the basal cochlear turn of these deaf mice by P30 [16]. Consistent with this conclusion, high frequency OHCs were shown to be particularly vulnerable to oxidative stress due to their elevated mitochondrial metabolism [67].

3.2. Accelerated presbycusis and increased oxidative stress in Gjb2$^{+/-}$ mice

In the subsequent set of experiments, we sought to determine whether oxidative stress affects auditory function also in heterozygous *Gjb2*$^{+/-}$ mice (Fig. 3). By measuring auditory brainstem responses (ABRs) to clicks and pure tone stimuli [29] at various ages (see Section 2), we found that hearing thresholds (Fig. 3A–C) estimated from Wave II amplitudes (Fig. 3D–F) were already slightly increased at 2 months of age (MoA) in *Gjb2*$^{+/-}$ mice compared to *Gjb2*$^{loxP/loxP}$ controls (Fig. 3A, D). At 6 MoA, the differences were significant for click responses and at 8, 16 and 32 kHz (Fig. 3B, E). By 12 MoA, also *Gjb2*$^{loxP/loxP}$ animals displayed signs of presbycusis, however hearing thresholds of *Gjb2*$^{+/-}$ mice remained significantly more elevated for click responses and

across the entire auditory spectrum examined (Fig. 3C, F). No differences were found between male and female *Gjb2*$^{+/-}$ and *Gjb2*$^{loxP/loxP}$ mice (Supplementary material, Fig. S1 and Table S1). Tg(Sox10-cre)1Wdr mice [14] and C57BL/6N mice (the genetic background shared by all animals in this study) showed a trend of age-related hearing loss in accord with a previous study which included C57BL/6N mice [68] and comparable to that of *Gjb2*$^{loxP/loxP}$ animals (Supplementary material, Fig. S2).

Measurement of distortion product otoacoustic emissions (DPOAE) [30,31] exhibited a significantly flatter growth function of the cubic (2f$_1$ − f$_2$) distortion product in *Gjb2*$^{+/-}$ mice at 2 and 6 MoA (Fig. 4), indicating that OHCs dysfunction contributed to the observed hearing impairment. These functional deficits correlated with a small but significant increase of OHC loss in *Gjb2*$^{+/-}$ cochleae at 6 MoA (Fig. 5A and Table 2). In addition, confocal immunofluorescence analysis of midmodiolar transversal sections revealed a dramatic flattening of the sensory epithelium in the outer sulcus region (Fig. 5B), as well as a significantly increased fraction of apoptotic nuclei in the organ of Corti of *Gjb2*$^{+/-}$ cochleae (Fig. 5C and Table 3). Tight junctions in the superficial layer of the cochlear sensory epithelium maintain cell polarity by providing a boundary between the apical and basolateral plasma membrane domains [69]. Therefore, these results suggest that diminished resistance to oxidative stress due to insufficient gap junction coupling might affect also tight junction stability, as reported in other systems [70,71].
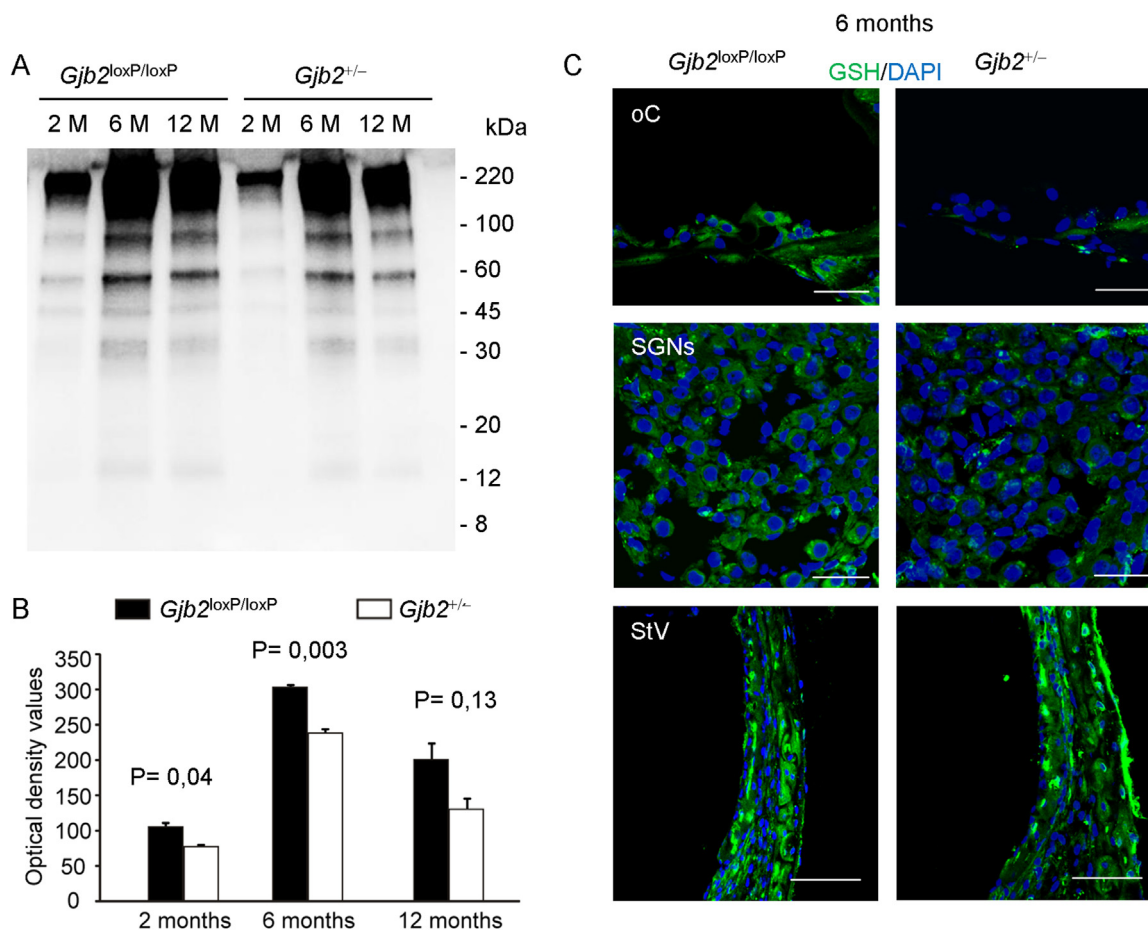
Fig. 9. Decreased levels of glutathionylated proteins in the cochlea of Gjb2$^{+/-}$ mice. A, B: Western blot analysis of glutathionylated proteins in Gjb2$^{loxP/loxP}$ and Gjb2$^{+/-}$ cochleae (n = 8 for each condition) at 2, 6 and 12 months of age (MoA). A: Representative immunoreactive bands showing a decrease of glutathionylated proteins at different molecular weights under non reducing conditions in Gjb2$^{+/-}$ mice. B: Quantitative analysis of optical density values evaluated at all molecular weights (mean ± s.e.m.). Experiments were performed in triplicate and p-values were determined by two-tailed t-test. C: Representative images of spiral ganglion neurons (SGNs), organ of Corti (oC) and *stria vascularis* (StV) with double labeling for GSH (green fluorescence) and DAPI staining (blue fluorescence) in Gjb2$^{loxP/loxP}$ and Gjb2$^{+/-}$ mice at 6 MoA. Scale bar: oC, 20 µm; SGNs, 30 µm; StV, 50 µm.

Degeneration of spiral ganglion neurons (SGNs), the first relay station of the afferent auditory pathway that conveys sensory information from organ of Corti hair cells to the central nervous system [72], is a hallmark of ARHL in mice [73]. As shown in Fig. 6, we detected loss of SGNs in Gjb2$^{+/-}$ mice due to significantly increased apoptosis at 6 and 12 MoA (Table 3 and Table 4; see also Supplementary material, Fig. S3 and Table S3). Staining of cochlear samples with DHE (Fig. 7A) and 4-HNE (Fig. 7B) revealed a time-dependent increase of both signals in the cochlear partition, *stria vascularis* and SGNs of Gjb2$^{+/-}$ mice at 2, 6 and 12 MoA. Quantitative image analysis showed that differences between cochlear tissue from Gjb2$^{+/-}$ mice and Gjb2$^{loxP/loxP}$ controls were significant at all 3 time points for DHE, but only at 6 MoA for 4-HNE. Together, these results confirm that apoptosis and accelerated presbycusis correlate with increased levels of oxidative stress in the cochlea of Gjb2$^{+/-}$ mice.

The Nrf2/ARE-controlled HO-1 enzyme, which contributes to redox homeostasis by catalyzing the oxidation of heme to biliverdin, free iron and carbon monoxide [20], has been previously implicated in protection of cochlear oxidative damage induced by noise exposure [32]. As shown in Fig. 8, we analyzed Nrf2 and HO-1 expression by western immunoblotting, and determined that levels of both markers were reduced in Gjb2$^{+/-}$ mice, compared to Gjb2$^{loxP/loxP}$ controls at 2 and 6 MoA and differences were significant at 6 MoA (Fig. 8A–C). To corroborate these findings, we performed image analysis of Nrf2 and HO-1 immunoreactivity in the cochlea at 6 MoA, and found reduced levels of

both markers in the organ of Corti, SGNs and *stria vascularis* of Gjb2$^{+/-}$ specimens (Fig. 8D). Finally we quantified the levels of cochlear glutathionylated proteins of different molecular weights under non reducing conditions by western blot analysis, and found significantly decreased levels of these proteins in Gjb2$^{+/-}$ specimens at 2, 6 MoA compared to age-matched Gjb2$^{loxP/loxP}$ controls (Fig. 9A, B). At 6 MoA, immunofluorescence analysis localized the decrease of glutathionylated proteins mainly in SGNs, organ of Corti, and *stria vascularis* (Fig. 9C).

In the brain, intercellular coupling via astrocytic gap junctions provides an activity-dependent intercellular pathway for the delivery of nutrients from blood vessels to distal neurons [74]. A similar role has been proposed for epithelial and connective tissue gap junction system of the cochlear duct [36], which are thought to supply sensory hair cells of the avascular sensory epithelium with nutrients derived from blood vessel networks in *stria vascularis*, spiral ligament and spiral limbus [75-77]. Nutrient deficiency impacts on ATP production, leading to ROS overload and apoptosis [78]. Therefore, we hypothesized that reduced expression of Cx26 in the cochlea of Gjb2$^{+/-}$ mice might promote oxidative damage by diminishing nutrient availability. To test this hypothesis, we used a non-metabolizable D-glucose analogue, 2-NBDG [35], as previously described [36]. As shown in Fig. 10, post-injection analysis of freshly dissected cochlear tissue revealed a significant reduction of 2-NBDG fluorescence emission in the *stria vascularis* of Gjb2$^{+/-}$ mice compared to age-matched Gjb2$^{loxP/loxP}$ controls.
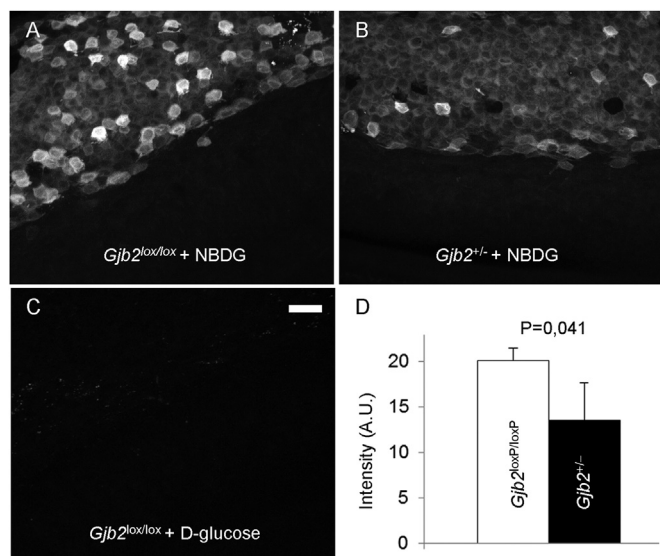
Fig. 10. 2-NBDG uptake and diffusion in the *stria vascularis* of Gjb2$^{+/-}$ mice. A–C: Representative fluorescence images of freshly dissected *stria vascularis* following injection of 2-NBDG (A, B) or ᴅ-glucose (C) dissolved in DPBS. Each image is the maximum fluorescence intensity projection of a through-focus sequence (z-stack, 20 frames, 2.0 μm increment) acquired with a customized two-photon microscope (see Section 2). Scale bar: 25 μm. D: Quantification of 2-NBDG fluorescence intensity (A.U., arbitrary units) in *stria vascularis* of Gjb2$^{loxP/loxP}$ and Gjb2$^{+/-}$ samples. Data are mean ± s.e.m. for m = 3 cochleae from n = 3 mice in each condition; p-values were determined by two-tailed t-test.

3.3. The Nrf2/ARE-pathway is altered in human cohorts with presbycusis

Together, the results presented above link causally development of presbycusis in Gjb2$^{+/-}$ mice, apoptosis and oxidative damage in the cochlear duct and spiral ganglion to reduced release of glutathione from connexin hemichannels, decreased nutrient delivery via cochlear gap junctions and deregulated expression of genes that are under transcriptional control of Nrf2.

In a recent work, a single nucleotide polymorphism (SNP, rs6721961) in the *NRF2* promoter, which reduces the transcription level of the *NRF2* gene, showed significant association with impaired hearing in a human cohort exposed to occupational noise [79]. This finding and the results described above prompted us to investigate whether genes in the NRF2/ARE-pathway show significant association with human hearing function and presbycusis traits. Thus, a GWAS analysis was carried out in a large cohort of 4091 individuals, originating from Europe, Caucasus and Central Asia, with hearing phenotype (including 1076 presbycusis patients and 1290 healthy matched controls). Analyzing normal hearing function traits (i.e. frequencies and thresholds thus a quantitative analysis) (**Analysis 1**, see Section 2), a statistically significant result was obtained at the 1 kHz hearing

threshold. In particular, 433 polymorphisms showed a p-value below nominal significance and one, rs7570049, located in *PRKCE* gene, was significantly associated after the Bonferroni correction (p-value = 2.20E-02). Analyzing the ARHL phenotype (i.e. cases vs. controls, thus a qualitative analysis; **Analysis 2**, see Section 2), 445 polymorphisms displayed a p-value below nominal significance threshold and four out of 445 were significantly associated after Bonferroni correction. Two polymorphisms (rs12613391, rs5839661) were located in *PRKCE* gene, while the remaining ones (rs12980839, rs8109627) in *TGFB1* gene. Interestingly, all five SNPs showed the same direction of the effect across all tested populations (beta value reported in Table 5), indicating an overall better hearing threshold (**Analysis 1**) and a reduced ARHL disease risk (**Analysis 2**) for carriers of the alternative allele thus suggesting a protective effect in the etiopathogenesis of presbycusis (Table 5).

Interestingly, one SNP (rs12980839) located within *TGFB1* gene is also included among the expression quantitative trait loci (eQTL) in the Genotype-Tissue Expression (GTEx) database [80]. Briefly, it shows a highly significant p-value (9.5×10^{-9}) indicating a decrease in gene tissue expression for homozygous subjects carrying the alternative allele compared to those with the reference allele. Overall, results from our population-based studies (i) show a statistically significant association with two genes (*PRKCE* and *TGFB1*) related to the NRF2 pathway (p-value $< 4 \times 10^{-2}$), (ii) further support the hypothesis that elements of the NRF2 pathway are essential for hearing maintenance and (iii) suggest that their dysfunction may play an important role in the etiopathogenesis of presbycusis.

4. Discussion

4.1. Consequences of targeted genetic ablation of Gjb2 in the epithelial gap junction system of the mouse cochlea

In the present study, we initially compared whole-genome expression profiles in the developing cochlea of Gjb2$^{-/-}$ mice, which fail to acquire hearing [16], to age-matched Gjb2$^{loxP/loxP}$ controls, which hear normally at 2 MoA and thereafter exhibit the same hearing loss progression of their genetic background (C57BL/6N; see Ref. [68] and Supplementary material, Figs. S1–2 and Tables S1–2). This search identified a total of 1733 genes with deregulated expression changes in P5 Gjb2$^{-/-}$ pups (Supplementary material, Data Set No.1). Functional enrichment analysis of deregulated genes (Supplementary material, Data Set No.2) showed that they were mainly involved in several processes, including MAPK signaling cascade, glutathione metabolism and antioxidant defense systems (Table 1 and Supplementary material, Data Set No.3), suggesting that these pathways may crosstalk with each other to drive hearing loss and cochlear degeneration. Our analysis also unveiled a number of differentially expressed genes associated to glutathione and/or oxidative metabolism, which are under transcriptional control of Nrf2. Disruption of Nrf2 signaling is associated with an increased susceptibility to oxidative insults and other toxicants in humans and model organisms [81-83]. In addition, this transcription factor has

Table 5
Results of candidate human gene association analyses. SNP: Analyzed polymorphism; Gene: Gene name; Chr: Chromosome; Position: Genomic position (GRCh37); Ref. Allele: Reference allele (allele reported in GRCh37); Alt. Allele: Alternative allele compared to the reference allele; N: Overall number of subjects considered in the analysis for the specific SNP; beta: Effect size – beta coefficient of the regression line, in which genotype at the SNP is used as a predictor of case-control status/ hearing threshold; p-value: P-value of the association test; Adjusted p-value: P-value of the association test, after the Bonferroni correction; An. Trait: Analyzed trait; HT: Hearing threshold at 1 kHz (quantitative trait regression analysis); Pres: Presbycusis (case-control analysis). See Section 2.

SNP	Gene	Chr	Position	Ref. Allele	Alt. Allele	N	beta	p-value	Adjusted p-value	An. trait
rs12613391	PRKCE	2	46,301,750	G	A	2366	− 0.080160009	5.87E − 05	2.61E − 02	Pres
rs58396617	PRKCE	2	46,303,933	G	A	2366	− 0.085993931	4.37E − 05	1.95E − 02	Pres
rs12980839	TGFB1	19	41,820,213	G	A	2366	− 0.05430617	9.51E − 05	4.23E − 02	Pres
rs8109627	TGFB1	19	41,822,986	T	C	2366	− 0.052945143	9.97E − 05	4.44E − 02	Pres
rs7570049	PRKCE	2	45,927,312	C	G	4091	− 0.01590765	5.07E − 05	2.20E − 02	HT

been recently identified as a key target for prevention of noise-induced oxidative damage and consequent hearing loss [79]. Increased levels of oxidative stress were detected also in C57BL/6J mice [84], the most frequently used animal model of presbycusis [85,68,86]. Furthermore, the senescence-accelerated mouse prone 8 (SAMP8) strain displays premature hearing loss and cochlear degeneration associated with oxidative stress, chronic inflammation and apoptotic cell death [87]. Thus, oxidative stress and alterations in the expression or function of Nrf2/ARE-controlled genes appear to contribute critically to the etiopathogenesis of hearing impairment in mouse models of deafness. On the basis of our results, we hypothesized that: (i) down-regulation of the glutathione synthetase GSHB could reduce glutathione production; (ii) down-regulation of the glutathione peroxidase GPX3 could reduce the transformation of GSH into GSSG; (iii) up-regulation of the glutathione S-transferase theta2 (GSTT2) could accelerate glutathione degradation; (iv) up-regulation of NOX4, an isoforms of nicotinamide adenine dinucleotide phosphate (NADPH) oxidase which is overexpressed also in neurons of an hypoxic mouse model, could contribute to an increased production of ROS [88-90].

4.2. Mechanisms underlying oxidative injury in the cochlea and the pathogenesis of presbycusis

Oxidative injury is a threshold phenomenon that occurs after antioxidant mechanisms are overwhelmed. In the brain, failure to cope generates oxidative injury that has been causally linked to loss of neurons during the progression of neurodegenerative diseases, such as Parkinson's disease, Alzheimer's disease and amyotrophic lateral sclerosis [91-94]. Protection of neurons from oxidative damage relies on Nrf2/ARE-mediated upregulation of the glial antioxidant response, which augments the synthesis of GSH [95]. Glial cells contribute to neuronal detoxification from ROS by releasing GSH [53] through plasma membrane hemichannels formed by Cx43 [54]. Our results indicate that cochlear nonsensory cells release GSH through hemichannels that contain Cx26 protomers.

Reduction of Cx26 expression in the mouse cochlea and alterations in the Nrf2/ARE pathway correlate with accelerated increase of hearing thresholds and lower DPOAE responses, as reported in Section 3. Moreover, the primary mechanism of regulation of NOX4 expression by Nrf2 in brain cells seems to be most likely indirect, i.e. determined by the levels of ROS, and so their level of expression could be regulated by a negative feedback loop [88]. This could explain why Nrf2 expression levels do not change significantly in $Gjb2^{-/-}$ mice at P5.

Based on our results with 2-NBDG, we suggest the following pathogenesis for the accelerated presbycusis of $Gjb2^{+/-}$ mice: (i) reduced gap junction coupling limits the transfer of nutrients, and glucose in particular, from distant blood vessels to the avascular sensory epithelium of the cochlea; (ii) glucose deprivation leads to oxidative stress; (iii) alterations in the Nrf2/ARE pathway and insufficient expression of Cx26 hemichannels limit the amount of detoxifying GSH released by cochlear non-sensory cells; (iv) prolonged exposure to oxidative stress causes lipid peroxydation which limits the function of GLUT transporters [96], further reducing the uptake of glucose by cochlear hair cells (vicious circle); (v) the elevated mitochondrial metabolism of OHCs [67], makes them particularly vulnerable to depletion of intracellular glucose levels.

From a molecular perspective, recent evidence suggests that glucose availability may regulate the NRF2-mediated antioxidant response through a dynamic nutrient-sensitive post-translational modification of KEAP1 and perhaps other substrates [97]. In addition, it has long been know that glucose-regulated protein 75 (GRP75) is induced under conditions of low glucose and other nutritional and environmental stresses [98]. This mitochondria-associated membrane (MAM) protein regulates ER–mitochondrial Ca^{2+} transfer [99] and has been recently shown to play a major role in sensitivity to oxidative stress in neuronal cells [100]. Our study suggests that these molecular players might be

also involved in the pathogenesis of the accelerated presbycusis.

4.3. Relevance of this study for human hearing

Presbycusis (or ARHL) is considered a polygenic and multifactorial disease with both genetic and environmental factors involved being largely unknown [101]. However, our results with a monogenic mouse model of hearing loss suggest that presbycusis might also arise from insufficient expression of Cx26, accompanied by increased levels of oxidative stress and deregulation of the Nrf2/ARE pathway in the cochlea. Of note, an ABR-based study reported hearing loss at frequencies in excess of 4 kHz in heterozygous (human) carriers of the *GJB2* 35delG variant [102]. Moreover, all carriers of one mutated *GJB2* allele had significantly lower DPOAEs across most frequencies, with a trend in the older age group towards lower DPOAEs [103,104]. Therefore our analysis offers a mechanistic explanation also for hearing loss in these subjects, based on augmented oxidative damage to SGNs, sensory and nonsensory (epithelial and supporting) cells.

Furthermore, results of our population based genetics studies in humans identified significant associations for two members of the Nrf2 pathway, namely *PRKCE* and *TGFB1,* a transforming growth factor whose protein regulates cell proliferation, differentiation and growth, and is frequently upregulated in tumor cells. Expression data available through the GTEx database lead to interesting findings for *TGFB1* indicating that subjects with a potential reduced ARHL risk (i.e. subjects carrying the alternative allele) might present a *TGFB1* decreased tissue expression. These findings suggest that *TGFB1* down-regulation in the $Gjb2^{-/-}$ animal models could play, at least in part, a protective compensative effect in these hearing impaired mice.

In summary, our results with a monogenic mouse model of hearing loss suggest that presbycusis might also arise from insufficient expression of the gap junction protein connexin 26 (Cx26) and highlight interesting candidates to be further validated in larger cohorts and with potential powerful translational opportunities. Therefore this work sheds new light on the etiopathogenesis of progressive hearing loss and also paves the way to its prevention in heterozygous carriers of 35deG, the prevalent *GJB2* mutation in several populations.

Author contributions

ARF: study conception, data quality control;
VZ, FP: collection of cochlear samples for microarray experiments, ABR and DPOAE recordings, immunofluorescence and immunoblotting, glucose injection experiments, statistical data analysis;
GZ, CP: post-glucose injection data collection and analyses.
MR, FS: mouse colony welfare, maintenance and genotyping;
AMS: data quality control;
GC: collection of cochlear samples for microarray experiments;
GT: analysis of DPOAEs data;
GG: microarray experiments, analysis and interpretation of genomic data;
AGS: bioinformatics data acquisition and statistical analyses;
DC: analysis of microarray results;

MG: microarray experiments;

GM: functional enrichment analysis of microarray results, edited the manuscript;

GVC, EF: supervision of GWAS data analysis;

MB: GWAS data analysis;

GG: GWAS data analysis, edited the manuscript

GP: data quality control;

PG: supervision of GWAS data analysis, edited the manuscript

SC: microarray data analysis direction and supervision, edited the manuscript;

FM: study conception, data quality control, wrote the manuscript.

Conflict of interest

The authors declare that the research was conducted in the absence of any commercial or financial relationships that could be construed as a potential conflict of interest.

Appendix A. Supplementary material

Supplementary data associated with this article can be found in the online version at doi:10.1016/j.redox.2018.08.002.

References

[1] A.A. Dror, K.B. Avraham, Hearing impairment: a panoply of genes and functions, Neuron 68 (2010) 293–308 https://www.sciencedirect.com/science/article/pii/S0896627310008354.

[2] F.J. Del Castillo, I. Del Castillo, DFNB1 Non-syndromic hearing impairment: diversity of mutations and associated phenotypes, Front. Mol. Neurosci. 10 (2017) 428 https://www.frontiersin.org/articles/10.3389/fnmol.2017.00428/full.

[3] D.P. Kelsell, J. Dunlop, H.P. Stevens, N.J. Lench, J.N. Liang, G. Parry, R.F. Mueller, I.M. Leigh, Connexin 26 mutations in hereditary non-syndromic sensorineural deafness, Nature 387 (1997) 80–83 https://www.nature.com/articles/387080a0.

[4] M.A. Kenna, H.A. Feldman, M.W. Neault, A. Frangulov, B.L. Wu, B. Fligor, H.L. Rehm, Audiologic phenotype and progression in GJB2 (connexin 26) hearing loss, Arch. Otolaryngol.–Head Neck Surg. 136 (2010) 81–87 https://www.ncbi.nlm.nih.gov/pmc/articles/PMC4528189/.

[5] R.L. Snoeckx, P.L. Huygen, D. Feldmann, S. Marlin, F. Denoyelle, J. Waligora, M. Mueller-Malesinska, A. Pollak, R. Ploski, A. Murgia, E. Orzan, P. Castorina, U. Ambrosetti, E. Nowakowska-Szyrwinska, J. Bal, W. Wiszniewski, A.R. Janecke, D. Nekahm-Heis, P. Seeman, O. Bendova, M.A. Kenna, A. Frangulov, H.L. Rehm, M. Tekin, A. Incesulu, H.H. Dahl, D. du Sart, L. Jenkins, D. Lucas, M. Bitner-Glindzicz, K.B. Avraham, Z. Brownstein, I. del Castillo, F. Moreno, N. Blin, M. Pfister, I. Sziklai, T. Toth, P.M. Kelley, E.S. Cohn, L. Van Maldergem, P. Hilbert, A.F. Roux, M. Mondain, L.H. Hoefsloot, C.W. Cremers, T. Lopponen, H. Lopponen, A. Parving, I. Schrijver, J. Roberson, F. Gualandi, A. Martini, G. Lina-Granade, N. Pallares-Ruiz, C. Correia, G. Fialho, K. Cryns, N. Hilgert, P. Van de Heyning, C.J. Nishimura, R.J. Smith, G. Van Camp, GJB2 mutations and degree of hearing loss: a multicenter study, Am. J. Hum. Genet. 77 (2005) 945–957 https://www.sciencedirect.com/science/article/pii/S0002929707633801.

[6] F. Denoyelle, D. Weil, M.A. Maw, S.A. Wilcox, N.J. Lench, D.R. Allen-Powell, A.H. Osborn, H.H. Dahl, A. Middleton, M.J. Houseman, C. Dode, S. Marlin, A. Boulila-ElGaied, M. Grati, H. Ayadi, S. BenArab, P. Bitoun, G. Lina-Granade, J. Godet, M. Mustapha, J. Loiselet, E. El-Zir, A. Aubois, A. Joannard, C. Petit, et al., Prelingual deafness: high prevalence of a 30delG mutation in the connexin 26 gene, Hum. Mol. Genet. 6 (1997) 2173–2177 https://academic.oup.com/hmg/article-pdf/6/12/2173/6956135/6-12-2173.pdf.

[7] L. Zelante, P. Gasparini, X. Estivill, S. Melchionda, L. D'Agruma, N. Govea, M. Mila, M.D. Monica, J. Lutfi, M. Shohat, E. Mansfield, K. Delgrosso, E. Rappaport, S. Surrey, P. Fortina, Connexin26 mutations associated with the most common form of non-syndromic neurosensory autosomal recessive deafness (DFNB1) in Mediterraneans, Hum. Mol. Genet. 6 (1997) 1605–1609 https://academic.oup.com/hmg/article/6/9/1605/2901425.

[8] S. Maeda, S. Nakagawa, M. Suga, E. Yamashita, A. Oshima, Y. Fujiyoshi, T. Tsukihara, Structure of the connexin 26 gap junction channel at 3.5 A resolution, Nature 458 (2009) 597–602 https://www.nature.com/articles/nature07869.

[9] S. Ortolano, G. Di Pasquale, G. Crispino, F. Anselmi, F. Mammano, J.A. Chiorini, Coordinated control of connexin 26 and connexin 30 at the regulatory and functional level in the inner ear, Proc. Natl. Acad. Sci. USA 105 (2008) 18776–18781 http://www.pnas.org/content/105/48/18776.long.

[10] T. Kikuchi, R.S. Kimura, D.L. Paul, J.C. Adams, Gap junctions in the rat cochlea: immunohistochemical and ultrastructural analysis, Anat. Embryol. 191 (1995) 101–118 https://link.springer.com/article/10.1007/BF00186783.

[11] H.D. Gabriel, D. Jung, C. Butzler, A. Temme, O. Traub, E. Winterhager, K. Willecke, Transplacental uptake of glucose is decreased in embryonic lethal connexin26-deficient mice, J. Cell Biol. 140 (1998) 1453–1461 http://jcb.rupress.org/content/jcb/140/6/1453.full.pdf.

[12] M. Cohen-Salmon, T. Ott, V. Michel, J.P. Hardelin, I. Perfettini, M. Eybalin, T. Wu, D.C. Marcus, P. Wangemann, K. Willecke, C. Petit, Targeted ablation of connexin26 in the inner ear epithelial gap junction network causes hearing impairment and cell death, Curr. Biol.: CB 12 (2002) 1106–1111 https://www.cell.com/current-biology/fulltext/S0960-9822(02)00904-1.

[13] Y. Wang, Q. Chang, W. Tang, Y. Sun, B. Zhou, H. Li, X. Lin, Targeted connexin26 ablation arrests postnatal development of the organ of Corti, Biochem. Biophys. Res. Commun. 385 (2009) 33–37 https://www.sciencedirect.com/science/article/pii/S0006291X09009115?via%3Dihub.

[14] T. Matsuoka, P.E. Ahlberg, N. Kessaris, P. Iannarelli, U. Dennehy, W.D. Richardson, A.P. McMahon, G. Koentges, Neural crest origins of the neck and shoulder, Nature 436 (2005) 347–355 https://www.nature.com/articles/nature03837.

[15] F. Anselmi, V.H. Hernandez, G. Crispino, A. Seydel, S. Ortolano, S.D. Roper, N. Kessaris, W. Richardson, G. Rickheit, M.A. Filippov, H. Monyer, F. Mammano, ATP release through connexin hemichannels and gap junction transfer of second messengers propagate Ca^{2+} signals across the inner ear, Proc. Natl. Acad. Sci. USA 105 (2008) 18770–18775 http://www.pnas.org/content/105/48/18770.

[16] G. Crispino, G. Di Pasquale, P. Scimemi, L. Rodriguez, F. Galindo Ramirez, R.D. De Siati, R.M. Santarelli, E. Arslan, M. Bortolozzi, J.A. Chiorini, F. Mammano, BAAV mediated GJB2 gene transfer restores gap junction coupling in cochlear organotypic cultures from deaf Cx26Sox10Cre mice, PLoS One 6 (2011) e23279 http://journals.plos.org/plosone/article?id=10.1371/journal.pone.0023279.

[17] S.L. Johnson, F. Ceriani, O. Houston, R. Polishchuk, E. Polishchuk, G. Crispino, V. Zorzi, F. Mammano, W. Marcotti, Connexin-mediated signaling in nonsensory cells is crucial for the development of sensory inner hair cells in the mouse Cochlea, J. Neurosci.: Off. J. Soc. Neurosci. 37 (2017) 258–268 http://www.jneurosci.org/content/37/2/258.full.pdf.

[18] A.R. Fetoni, P.M. Picciotti, G. Paludetti, D. Troiani, Pathogenesis of presbycusis in animal models: a review, Exp. Gerontol. 46 (2011) 413–425 https://www.sciencedirect.com/science/article/pii/S053155651000450X?via%3Dihub.

[19] Q. Huang, J. Tang, Age-related hearing loss or presbycusis, Eur. Arch. Oto-Rhino-Laryngol.: Off. J. Eur. Fed. Oto-Rhino-Laryngol. Soc. 267 (2010) 1179–1191 https://link.springer.com/article/10.1007/s00405-010-1270-7.

[20] Q. Ma, Role of nrf2 in oxidative stress and toxicity, Annu. Rev. Pharmacol. Toxicol. 53 (2013) 401–426 https://www.annualreviews.org/doi/pdf/10.1146/annurev-pharmtox-011112-140320.

[21] I. Buendia, P. Michalska, E. Navarro, I. Gameiro, J. Egea, R. Leon, Nrf2-ARE pathway: an emerging target against oxidative stress and neuroinflammation in neurodegenerative diseases, Pharmacol. Ther. 157 (2016) 84–104 https://www.sciencedirect.com/science/article/pii/S0163725815002168.

[22] H. Zhang, K.J.A. Davies, H.J. Forman, Oxidative stress response and Nrf2 signaling in aging, Free Radic. Biol. Med. 88 (2015) 314–336 https://www.sciencedirect.com/science/article/pii/S0891584915002592.

[23] H.K. Tabor, N.J. Risch, R.M. Myers, Candidate-gene approaches for studying complex genetic traits: practical considerations, Nat. Rev. Genet. 3 (2002) 391–397 https://www.nature.com/articles/nrg796.

[24] M Raess, AA de Castro, V Gailus-Durner, S Fessele, M Hrabě de Angelis, the IC., J. Jonkers, F. Iraqi, M.H. De Angelis, INFRAFRONTIER: a European resource for studying the functional basis of human disease, Mammalian Genome 27 (2016) 445–450 https://link.springer.com/content/pdf/10.1007%2Fs00335-016-9642-y.pdf.

[25] M. Ashburner, C.A. Ball, J.A. Blake, D. Botstein, H. Butler, J.M. Cherry, A.P. Davis, K. Dolinski, S.S. Dwight, J.T. Eppig, M.A. Harris, D.P. Hill, L. Issel-Tarver, A. Kasarskis, S. Lewis, J.C. Matese, J.E. Richardson, M. Ringwald, G.M. Rubin, G. Sherlock, Gene ontology: tool for the unification of biology. The Gene Ontology Consortium, Nat. Genet. 25 (2000) 25–29 https://www.nature.com/articles/ng0500_25.

[26] S. Ekins, Y. Nikolsky, A. Bugrim, E. Kirillov, T. Nikolskaya, Pathway mapping tools for analysis of high content data, Methods Mol. Biol. 356 (2007) 319–350 https://link.springer.com/protocol/10.1385/1-59745-217-3:319.

[27] H. Mi, X. Huang, M. Muruganujan, H. Tang, C. Mills, D. Kang, P.D. Thomas, PANTHER version 11: expanded annotation data from gene ontology and reactome pathways, and data analysis tool enhancements, Nucleic Acids Res. 45 (2017) D183–D189 https://academic.oup.com/nar/article/45/D1/D183/2605815.

[28] The Gene Ontology Consortium, Expansion of the Gene Ontology knowledgebase and resources, Nucleic Acids Res. 45 (2017) D331–D338 https://academic.oup.com/nar/article/45/D1/D331/2605810.

[29] P. Scimemi, R. Santarelli, A. Selmo, F. Mammano, Auditory brainstem responses to clicks and tone bursts in C57 BL/6J mice, Acta Otorhinolaryngol. Ital.: Organo Uff. della Soc. Ital. Otorinolaringol. Chir. cervico-facciale 34 (2014) 264–271 https://www.ncbi.nlm.nih.gov/pmc/articles/PMC4157533/pdf/0392-100X-34-264.pdf.

[30] P. Hofstetter, D. Ding, N. Powers, R.J. Salvi, Quantitative relationship of carboplatin dose to magnitude of inner and outer hair cell loss and the reduction in distortion product otoacoustic emission amplitude in chinchillas, Hear. Res. 112 (1997) 199–215 https://www.sciencedirect.com/science/article/pii/S0378595597001238.

[31] D.T. Kemp, Stimulated acoustic emissions from within the human auditory system, J. Acoust. Soc. Am. 64 (1978) 1386–1391 https://asa.scitation.org/doi/abs/10.1121/1.382104.

[32] A.R. Fetoni, F. Paciello, R. Rolesi, S.L. Eramo, C. Mancuso, D. Troiani, G. Paludetti, Rosmarinic acid up-regulates the noise-activated Nrf2/HO-1 pathway and protects against noise-induced injury in rat cochlea, Free Radic. Biol. Med. 85 (2015) 269–281 https://www.sciencedirect.com/science/article/pii/S0891584915001847.

[33] A.R. Fetoni, R. Rolesi, F. Paciello, S.L.M. Eramo, C. Grassi, D. Troiani, G. Paludetti, Styrene enhances the noise induced oxidative stress in the cochlea and affects differently mechanosensory and supporting cells, Free Radic. Biol. Med. 101 (2016) 211–225 https://www.sciencedirect.com/science/article/pii/S0891584916304841.

[34] A.R. Fetoni, P. De Bartolo, S.L. Eramo, R. Rolesi, F. Paciello, C. Bergamini, R. Fato, G. Paludetti, L. Petrosini, D. Troiani, Noise-induced hearing loss (NIHL) as a target of oxidative stress-mediated damage: cochlear and cortical responses after an increase in antioxidant defense, J. Neurosci. 27 (2013) 4011–4023 http://www.jneurosci.org/content/33/9/4011.full-text.pdf.

[35] C. Zou, Y. Wang, Z. Shen, 2-NBDG as a fluorescent indicator for direct glucose uptake measurement, J. Biochem. Biophys. Methods 64 (2005) 207–215 https://www.sciencedirect.com/science/article/pii/S0165022X05001260.

[36] Q. Chang, W. Tang, S. Ahmad, B. Zhou, X. Lin, Gap junction mediated intercellular metabolite transfer in the cochlea is compromised in connexin30 null mice, PLoS One 3 (2008) e4088 http://journals.plos.org/plosone/article?id=10.1371/journal.pone.0004088.

[37] M. Mezzavilla, D. Vozzi, N. Pirastu, G. Girotto, P. d'Adamo, P. Gasparini, V. Colonna, Genetic landscape of populations along the Silk Road: admixture and migration patterns, BMC Genet. 15 (2014) 131 https://bmcgenet.biomedcentral.com/articles/10.1186/s12863-014-0131-6.

[38] L. Van Laer, J.R. Huyghe, S. Hannula, E. Van Eyken, D.A. Stephan, E. Maki-Torkko, P. Aikio, E. Fransen, A. Lysholm-Bernacchi, M. Sorri, M.J. Huentelman, G. Van Camp, A genome-wide association study for age-related hearing impairment in the Saami, Eur. J. Hum. Genet.: EJHG 18 (2010) 685–693 https://www.nature.com/articles/ejhg2009234.

[39] D. Vuckovic, S. Dawson, D.I. Scheffer, T. Rantanen, A. Morgan, M. Di Stazio, D. Vozzi, T. Nutile, M.P. Concas, G. Biino, L. Nolan, A. Bahl, A. Loukola, A. Viljanen, A. Davis, M. Ciullo, D.P. Corey, M. Pirastu, P. Gasparini, G. Girotto, Genome-wide association analysis on normal hearing function identifies PCDH20 and SLC28A3 as candidates for hearing function and loss, Hum. Mol. Genet. 24 (2015) 5655–5664 https://academic.oup.com/hmg/article/24/19/5655/584102.

[40] D. Vuckovic, G. Biino, F. Panu, M. Pirastu, P. Gasparini, G. Girotto, Age related hearing loss and level of education: an epidemiological study on a large cohort of isolated populations, Hear. Balance Commun. 12 (2014) 94–98 https://www.tandfonline.com/doi/abs/10.3109/21695717.2014.911472.

[41] R.A. Friedman, L. Van Laer, M.J. Huentelman, S.S. Sheth, E. Van Eyken, J.J. Corneveaux, W.D. Tembe, R.F. Halperin, A.Q. Thorburn, S. Thys, S. Bonneux, E. Fransen, J. Huyghe, I. Pyykko, C.W. Cremers, H. Kremer, I. Dhooge, D. Stephens, E. Orzan, M. Pfister, M. Bille, A. Parving, M. Sorri, P.H. Van de Heyning, L. Makmura, J.D. Ohmen, F.H. Linthicum Jr., J.N. Fayad, J.V. Pearson, D.W. Craig, D.A. Stephan, G. Van Camp, GRM7 variants confer susceptibility to age-related hearing impairment, Hum. Mol. Genet. 18 (2009) 785–796 https://academic.oup.com/hmg/article/18/4/785/602424.

[42] G. Girotto, N. Pirastu, R. Sorice, G. Biino, H. Campbell, A.P. d'Adamo, N.D. Hastie, T. Nutile, O. Polasek, L. Portas, I. Rudan, S. Ulivi, T. Zemunik, A.F. Wright, M. Ciullo, C. Hayward, M. Pirastu, P. Gasparini, Hearing function and thresholds: a genome-wide association study in European isolated populations identifies new loci and pathways, J. Med. Genet. 48 (2011) 369–374 https://jmg.bmj.com/content/48/6/369.

[43] O. Delaneau, J. Marchini, J.F. Zagury, A linear complexity phasing method for thousands of genomes, Nat. Methods 9 (2011) 179–181 https://www.nature.com/articles/nmeth.1785.

[44] B.N. Howie, P. Donnelly, J. Marchini, A flexible and accurate genotype imputation method for the next generation of genome-wide association studies, PLoS Genet. 5 (2009) e1000529 http://journals.plos.org/plosgenetics/article?id=10.1371/journal.pgen.1000529.

[45] C. Genomes Project, G.R. Abecasis, A. Auton, L.D. Brooks, M.A. DePristo, R.M. Durbin, R.E. Handsaker, H.M. Kang, G.T. Marth, G.A. McVean, An integrated map of genetic variation from 1,092 human genomes, Nature 491 (2012) 56–65 https://www.nature.com/articles/nature11632.

[46] Y.S. Aulchenko, S. Ripke, A. Isaacs, C.M. van Duijn, GenABEL: an R library for genome-wide association analysis, Bioinformatics 23 (2007) 1294–1296 https://academic.oup.com/bioinformatics/article/23/10/1294/198080.

[47] C.J. Willer, Y. Li, G.R. Abecasis, METAL: fast and efficient meta-analysis of genomewide association scans, Bioinformatics 26 (2010) 2190–2191 https://academic.oup.com/bioinformatics/article/26/17/2190/198154.

[48] Student, The probable error of a mean, Biometrika 6 (1908) 1–25 https://www.jstor.org/stable/2331554?seq=1#page_scan_tab_contents.

[49] J.W. Tukey, Comparing individual means in the analysis of variance, Biometrics 5 (1949) 99–114 https://www.jstor.org/stable/3001913?seq=1#page_scan_tab_contents.

[50] H.B. Mann, D.R. Whitney, On a test of whether one of two random variables is stochastically larger than the other, Ann. Math. Stat. 18 (1947) 50–60 https://projecteuclid.org/euclid.aoms/1177730491.

[51] H.J. Forman, H. Zhang, A. Rinna, Glutathione: overview of its protective roles, measurement, and biosynthesis, Mol. Asp. Med. 30 (2009) 1–12 https://www.sciencedirect.com/science/article/pii/S0098299708000617.

[52] X. Jiang, J. Chen, A. Bajic, C. Zhang, X. Song, S.L. Carroll, Z.L. Cai, M. Tang, M. Xue, N. Cheng, C.P. Schaaf, F. Li, K.R. MacKenzie, A.C.M. Ferreon, F. Xia, M.C. Wang, M. Maletic-Savatic, J. Wang, Quantitative real-time imaging of glutathione, Nat. Commun. 8 (2017) 16087 https://www.nature.com/articles/ncomms16087.

[53] A.Y. Shih, D.A. Johnson, G. Wong, A.D. Kraft, L. Jiang, H. Erb, J.A. Johnson, T.H. Murphy, Coordinate regulation of glutathione biosynthesis and release by Nrf2-expressing glia potently protects neurons from oxidative stress, J. Neurosci.:

[54] Off. J. Soc. Neurosci. 23 (2003) 3394–3406 http://www.jneurosci.org/content/23/8/3394.long.

[54] S. Rana, R. Dringen, Gap junction hemichannel-mediated release of glutathione from cultured rat astrocytes, Neurosci. Lett. 415 (2007) 45–48 https://www.sciencedirect.com/science/article/pii/S0304394006013589.

[55] C. Rio, P. Dikkes, M.C. Liberman, G. Corfas, Glial fibrillary acidic protein expression and promoter activity in the inner ear of developing and adult mice, J. Comp. Neurol. 442 (2002) 156–162 https://onlinelibrary.wiley.com/doi/abs/10.1002/cne.10085.

[56] P. Majumder, G. Crispino, L. Rodriguez, C.D. Ciubotaru, F. Anselmi, V. Piazza, M. Bortolozzi, F. Mammano, ATP-mediated cell-cell signaling in the organ of Corti: the role of connexin channels, Purinergic Signal 6 (2010) 167–187 https://link.springer.com/article/10.1007/s11302-010-9192-9.

[57] L. Rodriguez, E. Simeonato, P. Scimemi, F. Anselmi, B. Cali, G. Crispino, C.D. Ciubotaru, M. Bortolozzi, F.G. Ramirez, P. Majumder, E. Arslan, P. De Camilli, T. Pozzan, F. Mammano, Reduced phosphatidylinositol 4,5-bisphosphate synthesis impairs inner ear Ca^{2+} signaling and high-frequency hearing acquisition, Proc. Natl. Acad. Sci. USA 109 (2012) 14013–14018 http://www.pnas.org/content/pnas/early/2012/08/08/1211869109.full.pdf.

[58] L. Xu, A. Carrer, F. Zonta, Z. Qu, P. Ma, S. Li, F. Ceriani, D. Buratto, G. Crispino, V. Zorzi, G. Ziraldo, F. Bruno, C. Nardin, C. Peres, F. Mazzarda, A.M. Salvatore, M. Raspa, F. Scavizzi, Y. Chu, S. Xie, X. Yang, J. Liao, X. Liu, W. Wang, S. Wang, G. Yang, R.A. Lerner, F. Mammano, Design and characterization of a human monoclonal antibody that modulates mutant connexin 26 hemichannels implicated in deafness and skin disorders, Front. Mol. Neurosci. 10 (2017) 298 https://www.frontiersin.org/articles/10.3389/fnmol.2017.00298/full.

[59] X. Tong W. Lopez J. Ramachandran W.A. Ayad Y. Liu A. Lopez-Rodriguez A.L. Harris J.E. Contreras Glutathione release through connexin hemichannels: implications for chemical modification of pores permeable to large molecules, J. Gen. Physiol. ⟨http://jgp.rupress.org/content/146/3/245.long⟩.

[60] I. Fasciani, A. Temperan, L.F. Perez-Atencio, A. Escudero, P. Martinez-Montero, J. Molano, J.M. Gomez-Hernandez, C.L. Paino, D. Gonzalez-Nieto, L.C. Barrio, Regulation of connexin hemichannel activity by membrane potential and the extracellular calcium in health and disease, Neuropharmacology (2013), https://www.sciencedirect.com/science/article/pii/S0028390813001366.

[61] V.K. Verselis, M. Srinivas, Divalent cations regulate connexin hemichannels by modulating intrinsic voltage-dependent gating, J. Gen. Physiol. 132 (2008) 315–327 http://jgp.rupress.org/content/132/3/315.short.

[62] L. Leybaert, P.D. Lampe, S. Dhein, B.R. Kwak, P. Ferdinandy, E.C. Beyer, D.W. Laird, C.C. Naus, C.R. Green, R. Schulz, Connexins in cardiovascular and neurovascular health and disease: pharmacological implications, Pharmacol. Rev. 69 (2017) 396–478 http://pharmrev.aspetjournals.org/content/69/4/396.long.

[63] L.I. Johnson-Cadwell, M.B. Jekabsons, A. Wang, B.M. Polster, D.G. Nicholls, 'Mild uncoupling' does not decrease mitochondrial superoxide levels in cultured cerebellar granule neurons but decreases spare respiratory capacity and increases toxicity to glutamate and oxidative stress, J. Neurochem. 101 (2007) 1619–1631 https://onlinelibrary.wiley.com/doi/abs/10.1111/j.1471-4159.2007.04516.x.

[64] J.D. West, L.J. Marnett, Alterations in gene expression induced by the lipid peroxidation product, 4-hydroxy-2-nonenal, Chem. Res. Toxicol. 18 (2005) 1642–1653 https://pubs.acs.org/doi/abs/10.1021/tx050211n.

[65] B. Teubner, V. Michel, J. Pesch, J. Lautermann, M. Cohen-Salmon, G. Sohl, K. Jahnke, E. Winterhager, C. Herberhold, J.P. Hardelin, C. Petit, K. Willecke, Connexin30 (Gjb6)-deficiency causes severe hearing impairment and lack of endocochlear potential, Hum. Mol. Genet. 12 (2003) 13–21 https://onlinelibrary.wiley.com/doi/abs/10.1111/j.1471-4159.2007.04516.x.

[66] A. Boulay, F.J. del Castillo, F. Giraudet, G. Hamard, C. Giaume, C. Petit, P. Avan, M. Cohen-Salmon, Hearing is normal without connexin30, J. Neurosci.: Off. J. Soc. Neurosci. 33 (2013) 430–434 http://www.jneurosci.org/content/33/2/430.

[67] H.C. Jensen-Smith, R. Hallworth, M.G. Nichols, Gentamicin rapidly inhibits mitochondrial metabolism in high-frequency cochlear outer hair cells, PLoS One 7 (2012) e38471 http://journals.plos.org/plosone/article?id=10.1371/journal.pone.0038471.

[68] K.L. Kane, C.M. Longo-Guess, L.H. Gagnon, D. Ding, R.J. Salvi, K.R. Johnson, Genetic background effects on age-related hearing loss associated with Cdh23 variants in mice, Hear. Res. 283 (2012) 80–88 https://www.sciencedirect.com/science/article/pii/S0378595511002838.

[69] E.R. Wilcox, Q.L. Burton, S. Naz, S. Riazuddin, T.N. Smith, B. Ploplis, I. Belyantseva, T. Ben-Yosef, N.A. Liburd, R.J. Morell, B. Kachar, D.K. Wu, A.J. Griffith, S. Riazuddin, T.B. Friedman, Mutations in the gene encoding tight junction claudin-14 cause autosomal recessive deafness DFNB29, Cell 104 (2001) 165–172 https://www.sciencedirect.com/science/article/pii/S0092867401002008.

[70] Y. Chi, X. Zhang, Z. Zhang, T. Mitsui, M. Kamiyama, M. Takeda, J. Yao, Connexin43 hemichannels contributes to the disassembly of cell junctions through modulation of intracellular oxidative status, Redox Biol. 9 (2016) 198–209 https://www.sciencedirect.com/science/article/pii/S2213231716301239.

[71] R. Rao, Oxidative stress-induced disruption of epithelial and endothelial tight junctions, Front. Biosci.: J. Virtual Libr. 13 (2008) 7210–7226 https://www.bioscience.org/2008/v13/af/3223/fulltext.htm.

[72] A.V. Bulankina, T. Moser, Neural circuit development in the mammalian cochlea, Physiology 27 (2012) 100–112 https://www.physiology.org/doi/pdf/10.1152/physiol.00036.2011.

[73] R.D. Frisina, B. Ding, X. Zhu, J.P. Walton, Age-related hearing loss: prevention of threshold declines, cell loss and apoptosis in spiral ganglion neurons, Aging 8 (2016) 2081–2099 http://www.aging-us.com/article/101045/text.

[74] N. Rouach, A. Koulakoff, V. Abudara, K. Willecke, C. Giaume, Astroglial metabolic

networks sustain hippocampal synaptic transmission, Science 322 (2008) 1551–1555 http://science.sciencemag.org/content/322/5907/1551.long.

[75] M. Ando, S. Takeuchi, Postnatal vascular development in the lateral wall of the cochlear duct of gerbils: quantitative analysis by electron microscopy and confocal laser microscopy, Hear. Res. 123 (1998) 148–156 https://www.sciencedirect.com/science/article/pii/S0378595598001099.

[76] M. Cohen-Salmon, S. Maxeiner, O. Kruger, M. Theis, K. Willecke, C. Petit, Expression of the connexin43- and connexin45-encoding genes in the developing and mature mouse inner ear, Cell Tissue Res. 316 (2004) 15–22 https://link.springer.com/article/10.1007%2Fs00441-004-0861-2.

[77] M. Cohen-Salmon, B. Regnault, N. Cayet, D. Caille, K. Demuth, J.P. Hardelin, N. Janel, P. Meda, C. Petit, Connexin30 deficiency causes instrastrial fluid-blood barrier disruption within the cochlear stria vascularis, Proc. Natl. Acad. Sci. USA 104 (2007) 6229–6234 http://www.pnas.org/content/104/15/6229.

[78] Y. Zhao, X. Hu, Y. Liu, S. Dong, Z. Wen, W. He, S. Zhang, Q. Huang, M. Shi, ROS signaling under metabolic stress: cross-talk between AMPK and AKT pathway, Mol. Cancer 16 (2017) 79 https://molecular-cancer.biomedcentral.com/articles/10.1186/s12943-017-0648-1.

[79] Y. Honkura, H. Matsuo, S. Murakami, M. Sakiyama, K. Mizutari, A. Shiotani, M. Yamamoto, I. Morita, N. Shinomiya, T. Kawase, Y. Katori, H. Motohashi, NRF2 is a key target for prevention of noise-induced hearing loss by reducing oxidative damage of cochlea, Sci. Rep. 6 (2016) 19329 https://www.nature.com/articles/srep19329.

[80] G.T. Consortium, The genotype-tissue expression (GTEx) project, Nat. Genet. 45 (2013) 580–585 https://www.nature.com/articles/ng.2653.

[81] Y. Aoki, H. Sato, N. Nishimura, S. Takahashi, K. Itoh, M. Yamamoto, Accelerated DNA adduct formation in the lung of the Nrf2 knockout mouse exposed to diesel exhaust, Toxicol. Appl. Pharmacol. 173 (2001) 154–160 https://www.sciencedirect.com/science/article/pii/S0041008X01991768.

[82] Y.J. Li, H. Takizawa, A. Azuma, T. Kohyama, Y. Yamauchi, S. Takahashi, M. Yamamoto, T. Kawada, S. Kudoh, I. Sugawara, Nrf2 is closely related to allergic airway inflammatory responses induced by low-dose diesel exhaust particles in mice, Clin. Immunol. 137 (2010) 234–241 https://www.sciencedirect.com/science/article/pii/S1521661610006819.

[83] G.P. Sykiotis, D. Bohmann, Stress-activated cap'n'collar transcription factors in aging and human disease, Sci. Signal. 3 (2010) re3 http://stke.sciencemag.org/content/3/112/re3.gloss.

[84] S. Someya, J. Xu, K. Kondo, D. Ding, R.J. Salvi, T. Yamasoba, P.S. Rabinovitch, R. Weindruch, C. Leeuwenburgh, M. Tanokura, T.A. Prolla, Age-related hearing loss in C57BL/6J mice is mediated by Bak-dependent mitochondrial apoptosis, Proc. Natl. Acad. Sci. USA 106 (2009) 19432–19437 http://www.pnas.org/content/106/46/19432.full.pdf.

[85] K.R. Johnson, L.C. Erway, S.A. Cook, J.F. Willott, Q.Y. Zheng, A major gene affecting age-related hearing loss in C57BL/6J mice, Hear. Res. 114 (1997) 83–92 https://www.sciencedirect.com/science/article/pii/S037859559700155X.

[86] K. Parham, Distortion product otoacoustic emissions in the C57BL/6J mouse model of age-related hearing loss, Hear. Res. 112 (1997) 216–234 https://www.sciencedirect.com/science/article/pii/S037859559700124X.

[87] J. Menardo, Y. Tang, S. Ladrech, M. Lenoir, F. Casas, C. Michel, J. Bourien, J. Ruel, G. Rebillard, T. Maurice, J.L. Puel, J. Wang, Oxidative stress, inflammation, and autophagic stress as the key mechanisms of premature age-related hearing loss in SAMP8 mouse cochlea, Antioxid. Redox Signal. 16 (2012) 263–274 https://www.liebertpub.com/doi/abs/10.1089/ars.2011.4037.

[88] S. Kovac, P.R. Angelova, K.M. Holmstrom, Y. Zhang, A.T. Dinkova-Kostova, A.Y. Abramov, Nrf2 regulates ROS production by mitochondria and NADPH oxidase, Biochim. Biophys. Acta 1850 (2015) 794–801 https://www.sciencedirect.com/science/article/pii/S0304416514003985.

[89] S. Pendyala, J. Moitra, S. Kalari, S.R. Kleeberger, Y. Zhao, S.P. Reddy, J.G. Garcia, V. Natarajan, Nrf2 regulates hyperoxia-induced Nox4 expression in human lung endothelium: identification of functional antioxidant response elements on the Nox4 promoter, Free Radic. Biol. Med. 50 (2011) 1749–1759 https://www.sciencedirect.com/science/article/pii/S0891584911001948.

[90] P. Vallet, Y. Charnay, K. Steger, E. Ogier-Denis, E. Kovari, F. Herrmann, J.P. Michel, I. Szanto, Neuronal expression of the NADPH oxidase NOX4, and its regulation in mouse experimental brain ischemia, Neuroscience 132 (2005) 233–238 https://www.sciencedirect.com/science/article/pii/S0306452205000308.

[91] K.J. Barnham, C.L. Masters, A.I. Bush, Neurodegenerative diseases and oxidative stress, Nat. Rev. Drug Discov. 3 (2004) 205–214 https://www.nature.com/articles/nrd1330.

[92] T.M. Dawson, V.L. Dawson, Molecular pathways of neurodegeneration in Parkinson's disease, Science 302 (2003) 819–822 http://science.sciencemag.org/content/302/5646/819.long.

[93] T. Finkel, N.J. Holbrook, Oxidants, oxidative stress and the biology of ageing, Nature 408 (2000) 239–247 https://www.nature.com/articles/35041687.

[94] W.R. Markesbery, Oxidative stress hypothesis in Alzheimer's disease, Free Radic. Biol. Med. 23 (1997) 134–147 https://www.sciencedirect.com/science/article/pii/S0891584996006296.

[95] A.Y. Shih, S. Imbeault, V. Barakauskas, H. Erb, L. Jiang, P. Li, T.H. Murphy, Induction of the Nrf2-driven antioxidant response confers neuroprotection during mitochondrial stress in vivo, J. Biol. Chem. 280 (2005) 22925–22936 http://www.jbc.org/content/280/24/22925.long.

[96] M.P. Mattson, Modification of ion homeostasis by lipid peroxidation: roles in neuronal degeneration and adaptive plasticity, Trends Neurosci. 21 (1998) 53–57 https://www.sciencedirect.com/science/article/pii/S0166223697011880.

[97] P.H. Chen, T.J. Smith, J. Wu, P.F. Siesser, B.J. Bisnett, F. Khan, M. Hogue, E. Soderblom, F. Tang, J.R. Marks, M.B. Major, B.M. Swarts, M. Boyce, J.T. Chi, Glycosylation of KEAP1 links nutrient sensing to redox stress signaling, EMBO J. 36 (2017) 2233–2250 http://emboj.embopress.org/content/36/15/2233.

[98] L.A. Mizzen, C. Chang, J.I. Garrels, W.J. Welch, Identification, characterization, and purification of two mammalian stress proteins present in mitochondria, grp 75, a member of the hsp 70 family and hsp 58, a homolog of the bacterial groEL protein, J. Biol. Chem. 264 (1989) 20664–20675 http://www.jbc.org/content/264/34/20664.full.pdf.

[99] C. Giorgi, A. Danese, S. Missiroli, S. Patergnani, P. Pinton, Calcium dynamics as a machine for decoding signals, Trends Cell Biol. 28 (2018) 258–273 https://www.sciencedirect.com/science/article/pii/S0962892418300023.

[100] B. Honrath, I. Metz, N. Bendridi, J. Rieusset, C. Culmsee, A.M. Dolga, Glucose-regulated protein 75 determines ER-mitochondrial coupling and sensitivity to oxidative stress in neuronal cells, Cell Death Discov. 3 (2017) 17076 https://www.nature.com/articles/cddiscovery201776.

[101] X.Z. Liu, D. Yan, Ageing and hearing loss, J. Pathol. 211 (2007) 188–197 https://onlinelibrary.wiley.com/doi/abs/10.1002/path.2102.

[102] A. Franze, A. Caravelli, F. Di Leva, E. Marciano, G. Auletta, F. D'Aulos, C. Saulino, L. Esposito, M. Carella, P. Gasparini, Audiometric evaluation of carriers of the connexin 26 mutation 35delG, Eur. Arch. Oto-Rhino-Laryngol.: Off. J. Eur. Fed. Oto-Rhino-Laryngol. Soc. 262 (2005) 921–924 https://link.springer.com/article/10.1007%2Fs00405-005-0918-1.

[103] B. Engel-Yeger, S. Zaaroura, J. Zlotogora, S. Shalev, Y. Hujeirat, M. Carrasquillo, S. Barges, H. Pratt, The effects of a connexin 26 mutation–35delG–on oto-acoustic emissions and brainstem evoked potentials: homozygotes and carriers, Hear. Res. 163 (2002) 93–100 https://www.sciencedirect.com/science/article/pii/S0378595501003860.

[104] B. Engel-Yeger, S. Zaaroura, J. Zlotogora, S. Shalev, Y. Hujeirat, M. Carrasquillo, B. Saleh, H. Pratt, Otoacoustic emissions and brainstem evoked potentials in compound carriers of connexin 26 mutations, Hear. Res. 175 (2003) 140–151 https://www.sciencedirect.com/science/article/pii/S0378595502007190.